ZIRAT-10 SPECIAL TOPICS REPORT

Impact of Irradiation on Material Performance

Prepared by

Ron Adamson
Zircology Plus, Fremont, California, USA

Brian Cox
University of Toronto, Ontario, Canada

October, 2005

Advanced Nuclear Technology International
Ekbacken 33
SE-735 35 SURAHAMMAR
Sweden

info@antinternational.com

DISCLAIMER

The information presented in this report has been compiled and analysed by Advanced Nuclear Technology International Europe AB (ANT International) and its subcontractors. ANT International has exercised due diligence in this work, but does not warrant the accuracy or completeness of the information. ANT International does not assume any responsibility for any consequences as a result of the use of the information for any party, except a warranty for reasonable technical skill, which is limited to the amount paid for this assignment by each ZIRAT program member.

FOREWORD

At the end of this report a conversion table appear providing conversion factors between SI and US units.

The personal viewpoints and conclusions presented in the report that are beyond those quoted from references, are those of the individual authors and may not represent the collective view of all authors.

Peter Rudling, Editor

CONTENTS

1 INTRODUCTION (RON ADAMSON)

1.1 OVERVIEW OF "IMPACT OF IRRADIATION ON MATERIALS PERFORMANCE"

Reactor neutron irradiation dramatically affects the properties and performance of all the materials in the reactor core. This special report focuses on the behaviour of zirconium alloys used for the main structural components in the fuel bundle. The ZIRAT Annual Report series reviews the zirconium alloy literature for a given year. The Special Topics Reports such as this one take a much broader view of the special topic and include all literature relevant to the topic, and depend on the experience of the ZIRAT authors to provide a balanced and insightful description of the topic.

This report covers five main technical areas. Section 2 addresses microstructures of zirconium alloys as affected by the intense flux of neutrons and other energetic particles associated with the nuclear fission process. Included are discussion of irradiation-induced point defects and dislocation loops, and dissolution of second phase precipitates in the zirconium matrix. Section 3 addresses the effects of irradiation on the range of characteristics important for material mechanical performance, including strength, ductility, deformation mechanisms, fatigue and fracture toughness. Section 4 addresses the important questions of dimensional stability of zirconium alloys, including irradiation growth and irradiation creep. Section 5 discusses the impact of irradiation on hydrogen solubility in Zr and its alloys. Section 6 addresses the influence of irradiation on corrosion behaviour of the various zirconium alloys, and relates some of that behaviour to the effects of microstructure discussed in Section 2. Finally, Section 7 provides recommendations of needed work related to the topics covered in this report.

This report should provide a solid understanding of the role that irradiation plays in component performance, and will be a complementary companion to the other ZIRAT 10 Special Topic Report on Structural Behavior of Fuel Components.

1.2 IRRADIATION DAMAGE UNITS

Performance of nuclear materials is often judged as a function of time in a reactor, or as a function of exposure to the reactor environment. To the materials analyst an important unit of exposure is neutron fluence, or the number of neutrons that have passed through a unit area of material, n/cm^2 or n/m^2. Since the amount of "damage" done by neutrons depends on the energy of the neutron, it is necessary to specify the neutron energy of record. Since more "damage" is done by high energy or "fast" neutrons, the most common unit is for neutron energies greater than 1 MeV, fluence ≡ n/m^2 (E>1 MeV).

However, sometimes a lower energy is noted, fluence ≡ n/m^2 E>0.1 MeV.

For light water reactors (BWR and PWR) a rule of thumb is that

$2\ n/m^2$ (E>0.1 MeV) is about $1\ n/m^2$ (E>1MeV).

However, for fast reactors of the BOR60 type used in Russia the relationship is closer to:

$$3.4\ n/m^2\ (E>0.1\ MeV) \text{ is about } 1\ n/m^2\ (E>1MeV).$$

Detailed comparisons, of course, must be based on detailed analysis of the neutron energy spectra of reactors of interest. If the complete energy spectrum is considered and consistent estimates of the neutron energy needed to "knock" an atom from its normal lattice position are used, it is helpful to use displacement per atom, dpa, as the measure of irradiation damage. DPA refers to the average number of times an individual atom is displaced from its normal lattice position during a given reactor exposure. For zirconium alloys in a typical light water reactor a value commonly used is:

$$1\ dpa = 4.5 \times 10^{24}\ n/m^2\ (E>1\ MeV).$$

This is reported by Fidleris et al., 1987, who used a threshold displacement energy of 25 eV. Other numbers are used, however.

Shishov et al., 2004 reports $6x10^{24}$ n/m^2, E>1MeV for 1 dpa using an unknown displacement energy.

It is clear that fluence comparisons from reactor to reactor are tricky, and relative errors or differences of 50% are possible. In test reactors it is common to measure fluence or flux through radioactivity analyses of flux wires or foils (Fe, Ni, Cu etc., ASTM Standard E260-03). In commercial reactors flux measurements are a standard part of reactor instrumentation.

For reactor engineers the most important unit of exposure is fuel burnup. This is usually expressed as

$$\text{exposure} \equiv \text{GWd/MT or MWd/KgU.}$$

The conversion of burnup to a neutron fluence is complex, depending on neutron-energy spectrum, fuel enrichment, void fraction and other factors. But for a rule of thumb, it is usually close to use:

$$10\ \text{GWd/MT is about } 2 \times 10^{25}\ n/m^2\ (E>1\ MeV).$$

It is therefore seen that an end-of-life exposure of

$$50\ \text{GWd/MT}$$

is equivalent to

$$1 \times 10^{26}\ n/m^2\ (E>1\ MeV)$$

or

$$20\ \text{dpa.}$$

This means that on the average each atom has been displaced from its normal lattice site about 20 times! No wonder properties are expected to change with reactor exposure.

In this report, unless otherwise stated fluence is reported for E>1 MeV.

2 MICROSTRUCTURE (RON ADAMSON)

2.1 EQUILIBRIUM

Under thermodynamic equilibrium, all metals contain a certain number of defects – vacancies, interstitials, dislocations.

2.1.1 Dislocations

When materials scientists first realized that metals consisted of a regular array of atoms arranged in planes, they were able to calculate the stress needed to cause one plane of atoms to move one atom position relative to the adjacent plane of atoms. The stress required was about 10^7 psi (69 000 MPa), which is at least 100X greater than observed experimentally. The concept of a lattice defect, the dislocation, was therefore introduced to explain the discrepancy. It was shown theoretically that a dislocation could move through the crystal lattice at far less than the theoretical stress, and that it would produce a slip step, or a shear step, at a free surface.

Although it is not important for the purposes of this special topic report to examine dislocation theory, it will be helpful to review some basic geometries and terms. As indicated in Figure 2-1, a dislocation can be envisioned as an extra plane of atoms in the lattice. Because the interatomic forces around the dislocation line are different than in a perfect lattice, the dislocation (in the illustrated case an edge dislocation) can move under the influence of an applied shear stress. When the edge dislocation reaches a free surface it does indeed cause a step at the surface. Figure 2-2, Dieter, 1961, illustrates the case of a dislocation, or group of dislocations, intersecting the surface of a copper single crystal. The basic phenomena are the same for Zircaloy.

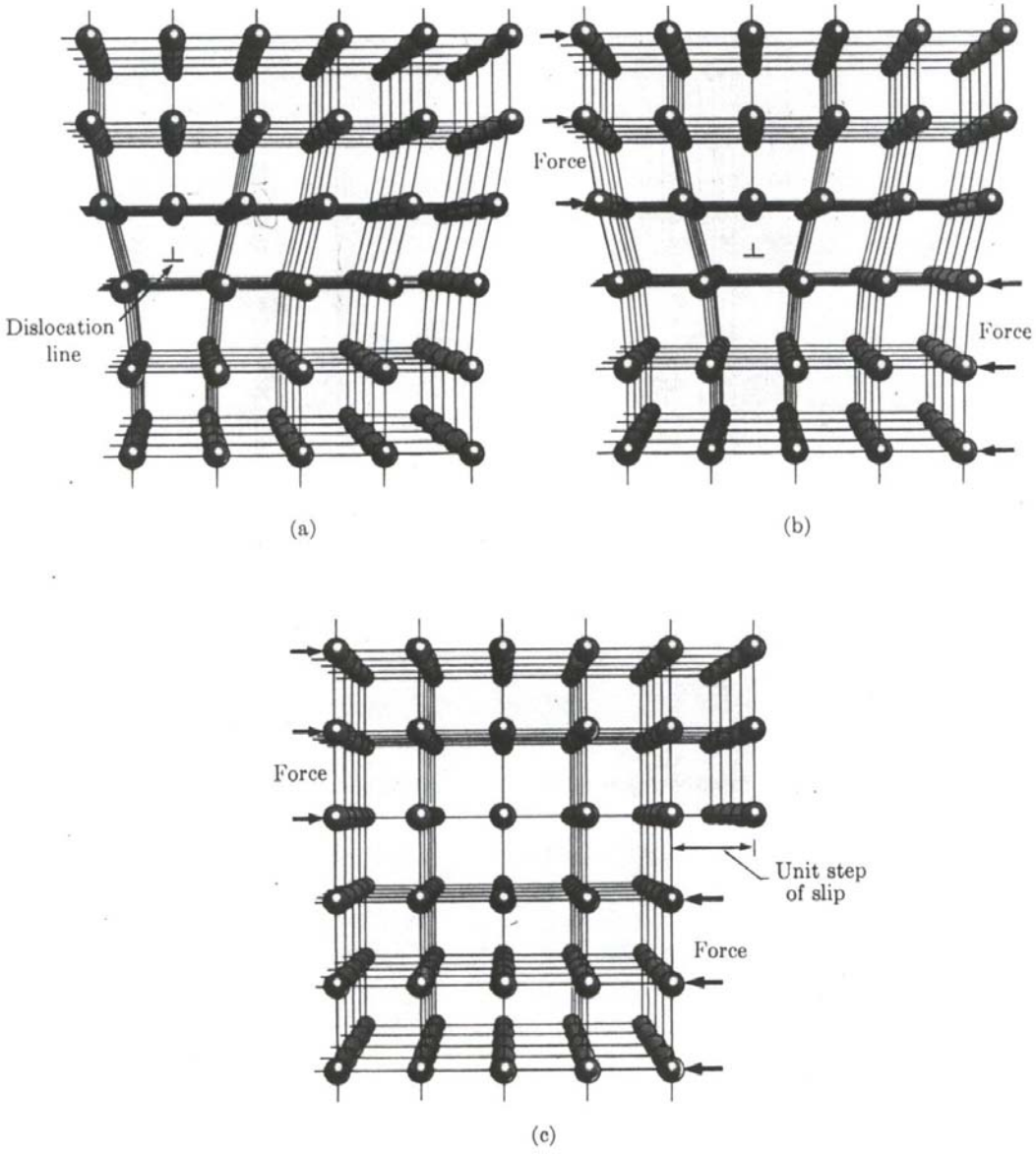

Figure 2-1: The motion of an edge dislocation and the production of a unit step of slip at the surface of the crystal. (a) An edge dislocation in a crystal structure. (b) The dislocation has moved one lattice spacing under the action of a shearing force. (c) The dislocation has reached the edge of the crystal and produced unit slip.

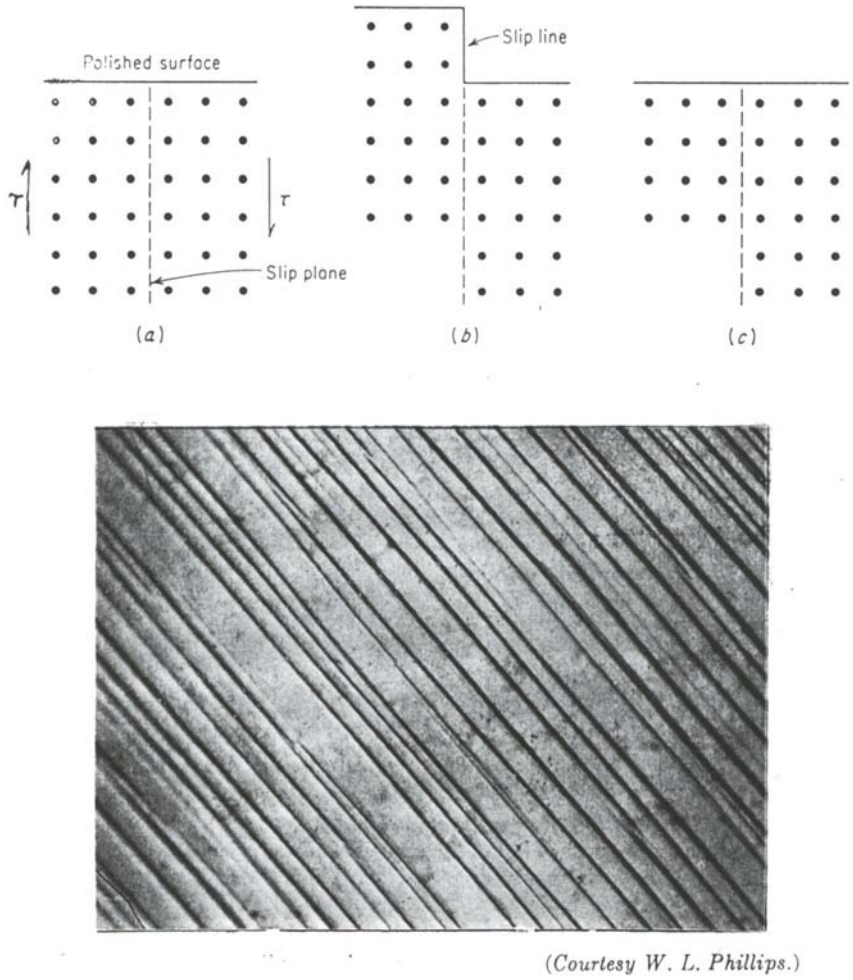

Figure 2-2: Schematic drawing of classical slip (above) and actual slip lines in copper, 500X (below), Dieter, 1961.

When describing deformation or irradiation-induced defects, the term Burgers vector (**b**) is often used. Figure 2-3, Weertman & Weertman, illustrates that b has a direction along the slip plane (perpendicular to the dislocation line in the case of an edge dislocation) and a magnitude close to that of one atomic spacing. If one takes a circuit around an atom in a perfect lattice, the circuit closes on itself, as in the lower portion of Figure 2-3. If a circuit is taken around an edge dislocation, the circuit does not close. The translation needed to close the circuit defines the Burgers vector, as in the upper portion of the figure. The Burgers vector helps characterize irradiation-produced defects, as will be discussed later.

It has been convincingly shown that dislocations exist in metals and other materials. An example is shown in Figure 2-4, Dieter, 1961, where crystal planes are revealed by transmission electron microscopy. In metals the density of dislocations in a fully recrystallized (soft) material is on the order of 10^8 cm^{-2} (cm/cm^3). Deformation causes the moving dislocations to interact, resulting in two effects: 1) multiplication of the dislocaton density, to about 10^{12} cm^{-2} in fully cold worked materials and 2) increase in the resistance to free motion of the dislocations and an accompanying increase in strength (work hardening).

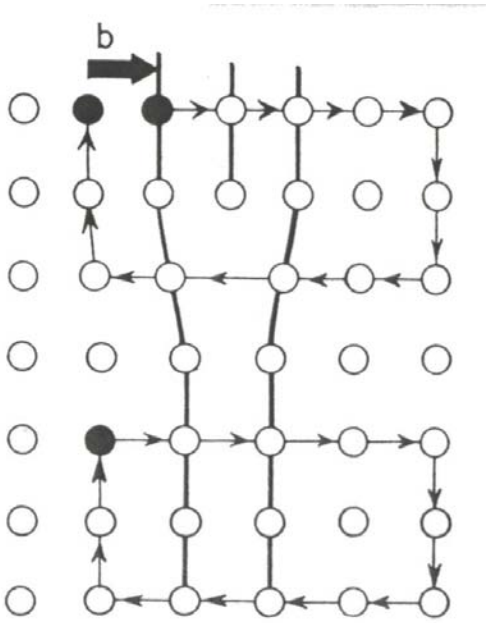

Figure 2-3: Burgers circuit around edge dislocation. The Burgers vector is b, Weertman & Weertman.

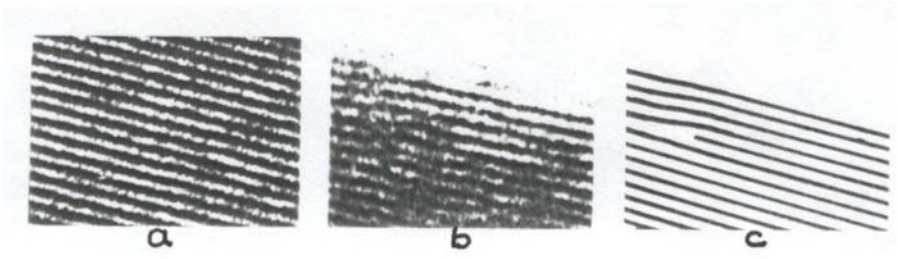

Figure 2-4: Electron Micrograph of dislocation in a crystal of plantinum phthalocyanine (X1,500,000). (a) Example of perfect array of crystal planes. (b) Perfect array interrupted by a dislocation. (c) Schematic drawing of (b) showing position of the dislocation, Dieter, 1961.

2.1.2 Point Defects

Another class of defects which is important to the understanding of mechanical properties is the point defect. Some types are illustrated in Figure 2-5, Dowling, 1999. A substitutional impurity occupies a normal lattice site but is an atom of a different element than the bulk material. A vacancy is the absence of an atom at a normally occupied lattice site, and an interstitial is an atom occupying a position between normal lattice sites. If the interstitial is of the same type as the bulk material, it is called a self interstitial and if it is of another kind it is called an impurity interstitial.

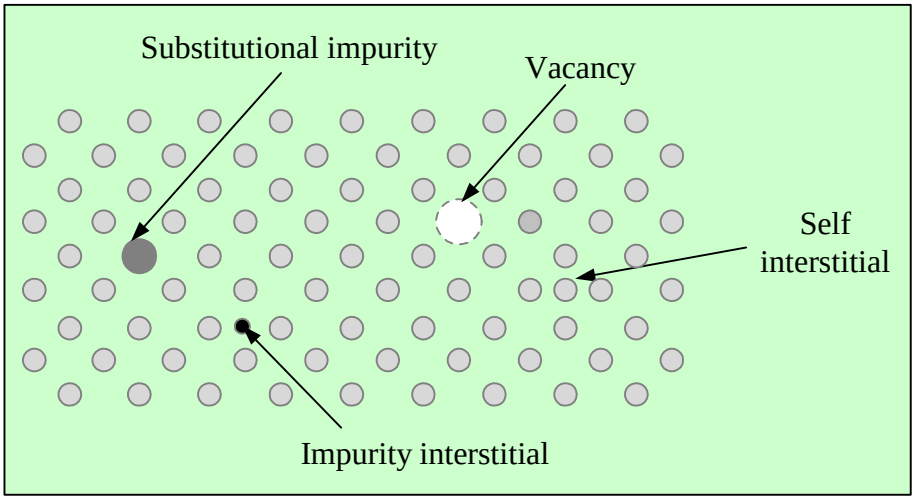

Figure 2-5: Four types of point defects, modified figure according to Dowling, 1999.

Relatively small impurity atoms often occupy interstitial sites in materials with larger atoms. In zirconium alloys common interstitials are O, H, C, Fe, Cr and Ni. Common substitutional impurities (or alloying elements) are Sn and Nb.

It is seen in Figure 2-1 that the region around an edge dislocation is under stress due to the disruption of the normal lattice spacing there. As a result, this region strongly attracts vacancies, interstitials and self interstitials. For instance, for temperatures around 573K (300°C), oxygen in zirconium is strongly attracted to dislocations, and significantly affects the strength of unirradiated materials.

2.1.3 Dislocation Loops

An important type of defect, particularly for irradiated materials, is the dislocation loop. If a significant number of vacancies or interstitials condense on a particular plane, a disk is formed with its boundary defined by a (circular) edge dislocation. This is illustrated in Figure 2-6 and Figure 2-7, Franklin et al., 1983. The Burgers vector b is perpendicular to the plane of the loop and therefore is the normal to the plane on which the loop lies.

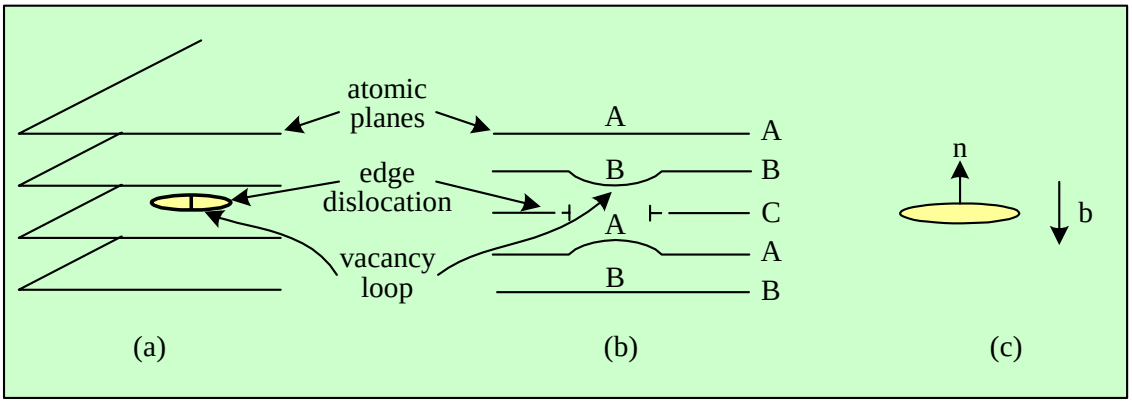

The vacancy loop: (a) Oblique view of a vacancy loop appearing as a disk on an atomic plane; (b) side view showing the change in stacking sequence through the loop; (c) orientation of the loop normal $\vec{n}$ to the Burgers vector $\vec{b}$.

Figure 2-6: Vacancy loop, modified figure according to Franklin et al., 1983.

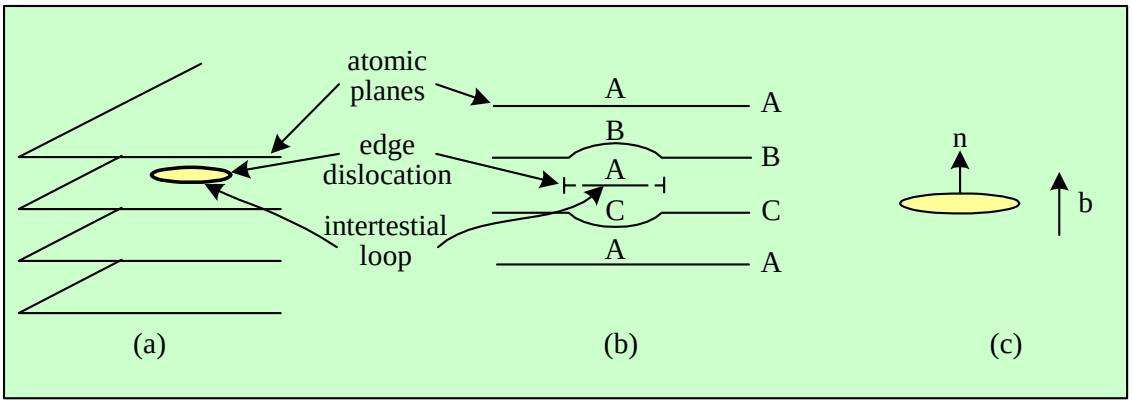

The interstitial loop: (a) Oblique view of a interstitial loop as a disk of atoms between atomic planes; (b) side view showing the change in stacking sequence; (c) orientation of the loop normal $\vec{n}$ to the Burgers vector $\vec{b}$.

Figure 2-7: Interstitial loop, modified figure according to Franklin et al., 1983.

2.2 TEXTURE

Deformation in zirconium (and titanium) alloys is unique among the common structural materials in that properties are anisotropic, that is they are different in each direction of the material or component. Fabrication techniques intensify these differences, but anisotropy is inherent to zirconium because of its crystal structure. The zirconium crystallography is hexagonal close packed (HCP), as shown in Figure 2-8. Whereas the ratio of the orthogonal crystallographic axes in cubic materials like steel, Inconel, brass, etc., is unity, in zirconium it is 1.59, with the c-axis larger than the a-axis. As a result, not only are mechanical properties such as strength and ductility anisotric, but also physical properties such as thermal expansion coefficients, thermal conductivity and elastic modulus. For the purposes of this review, the most important planes (noted in Figure 2-8) are two orthogonal planes, basal {0001} and prism $\{0\bar{1}10\}$, and a plane inclined to both of the above, pyramidal $\{01\bar{1}2\}$, where the brackets {….} represent a family of planes.

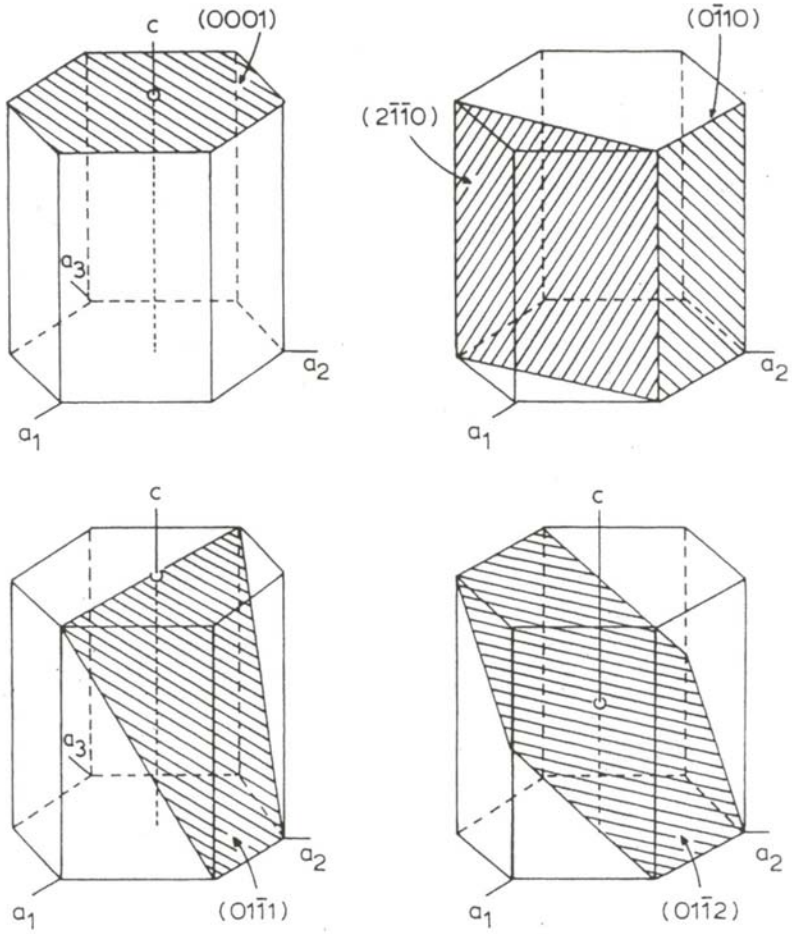

Figure 2-8: Some important planes in the hcp system in their Miller-Bravais indices. Prism planes $(0\bar{1}10)$. Pyramidal $(01\bar{1}2)$ or $(01\bar{1}1)$. Basal (0001).

To enable the degree of anisotropy to be predicted, the texture (i.e., arrangement of crystallographic planes) of a specimen or component is usually expressed as an average distribution of basal (0001) planes in a particular direction of interest. X-ray diffraction techniques are used to obtain this distribution or the distribution of any plane of interest, Lewis, et al., 1982. Figure 2-9, Schemel, 1989, shows the distribution of basal poles (normals to the basal plane) in various circumstances, with the usual distribution in Zircaloy tubing shown in Figure 2-9(e). More quantitatively, the distribution of basal poles is expressed by the Kearns texture parameter, f_x, where f_x is the resolved volumn fraction of basal poles lying in the x-direction. The following definitions apply:

- f_l = longitudinal (rolling, axial) direction
- f_t = transverse (circumferential) direction
- f_n = normal (radial) direction
- $f_l + f_t + f_n = 1$
- f = 0.33 implies randomly oriented basal poles.

In Figure 2-9(b), $f_l = f_n = 0$ and $f_t = 1$

In Figure 2-9(d), $f_l = f_t = 0$ and $f_n = 1$

In Figure 2-9(c), $f_l = f_n = f_t = .33$

In Figure 2-9 (e), showing a typical texture in Zircaloy tubing, $f_l = 0.07$, $f_t = 0.33$, $f_n = 0.60$

In a typical rolled plate $f_l = .1$, $f_t = .3$, $f_n = .6$.

A detailed account of texture-related deformation in zirconium alloys is given by Tenckhoff, 1988, a summary of which is given in Rudling & Adamson, 2000.

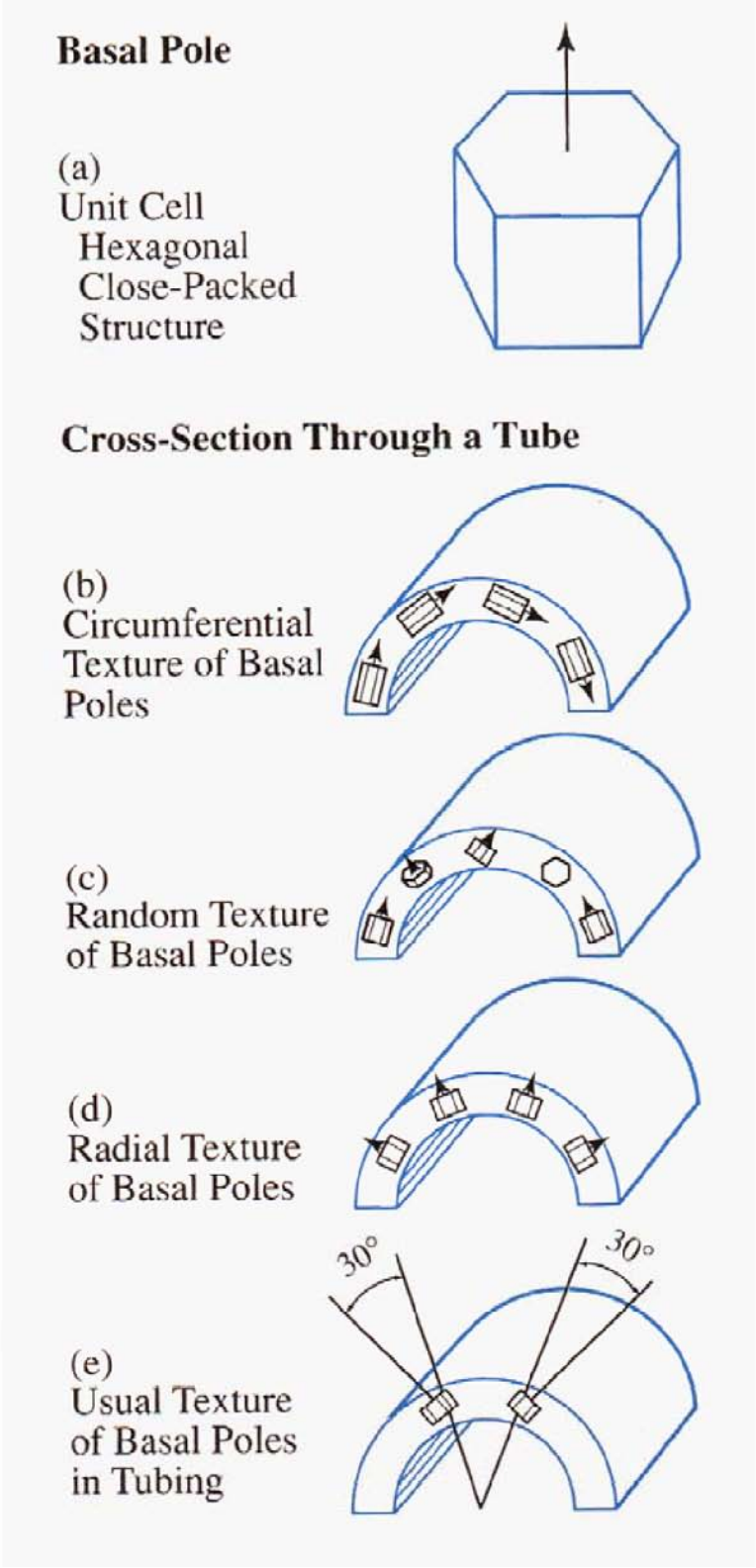

Figure 2-9: Illustration of crystal textures in tubing, Schemel, 1989.

2.3 IRRADIATION DAMAGE

2.3.1 General

Under irradiation, many more defects are created by elastic and non-elastic collisions between the radiation particles and irradiated metal. The most simple type of irradiation-produced defect is the Frenkel pair, which is the vacancy-interstitial pair that is formed when an atom is knocked from its normal lattice position (forming a vacancy) and lodges itself in an interstitial position nearby in the lattice (forming a self-interstitial). A more complicated but transient form of damage results when many atoms are displaced locally, shown in Figure 2-10, Chalmers, 1959 as a displacement spike (which is a form of what is sometimes termed a thermal spike). In this case many atoms have been forced into interstitial sites surrounding a hollow core. This configuration is not stable, however, and quickly converts to the situation shown in Figure 2-11, Franklin et al., 1983, which is a damage zone with a vacancy rich core and an interstitial shell. This configuration is also not stable, as the vacancies and interstitials prefer to migrate to sinks such as grain boundaries and dislocations. Importantly, many of the vacancies combine together in planar arrays to form the vacancy dislocation loops shown in Figure 2-6, and the interstitials do likewise to form interstitial dislocation loops, Figure 2-7.

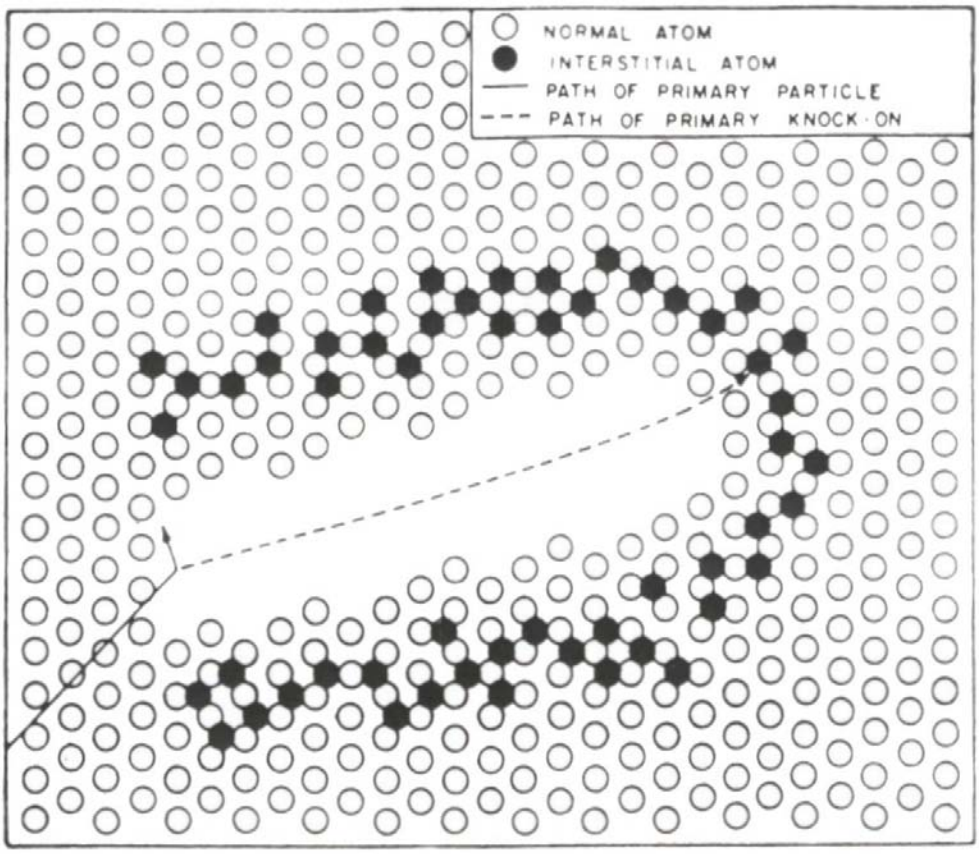

Figure 2-10: Schematic drawing of a (Brinkman) displacement spike, Chalmers, 1959.

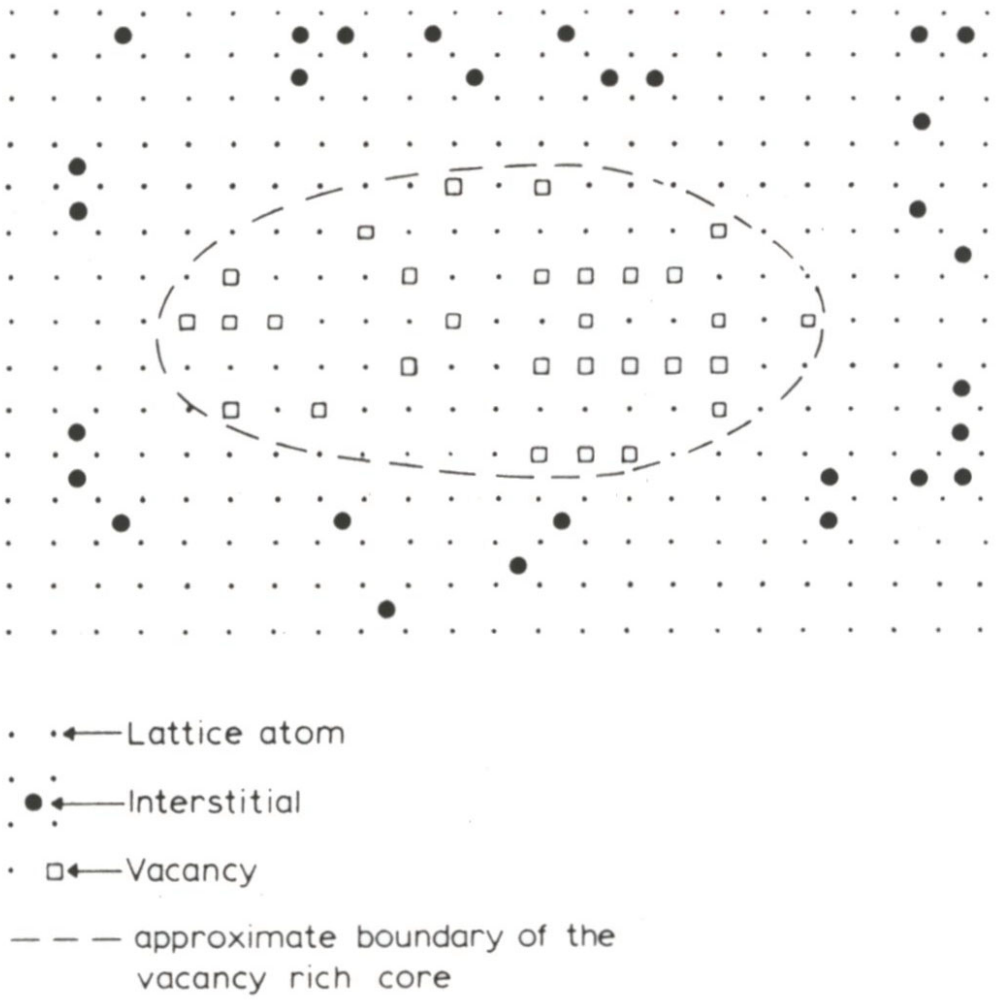

Figure 2-11: Illustration of a damage zone with a vacancy rich core and an interstitial shell, Franklin et al., 1983.

In a reactor environment, defects are potentially produced by neutrons, beta particles (electrons), alpha partricles and gamma rays (γ-rays). The types of defects produced by each is illustrated in Figure 2-12, Van Bueren, 1961. Neutrons and alpha particles cause the most damage per particle, but because of its electrical charge alphas have a very short range in metals. Electrons and gammas have a large range in metals, but cause very few defects, mainly isolated Frenkel pairs.

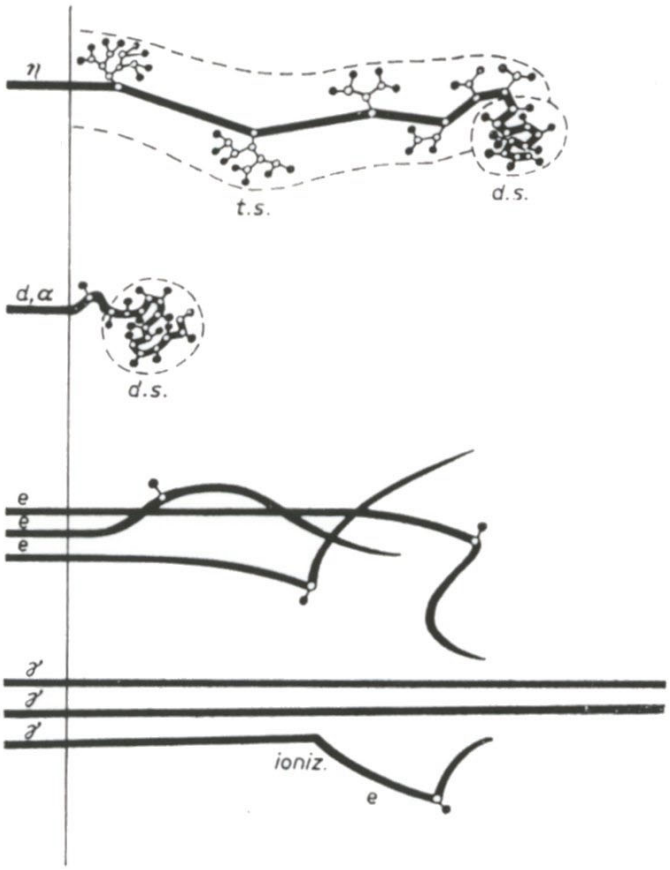

Schematic comparison between the results of different sorts of fast-particle irradiation of solids. Neutrons (n) produce localized clusters of many (about 100) Frenkel defects, together with thermal spikes of great relative importance for the total damage. Charged particles such as deuterons (d) or alpha particles (α) cause less damage than neutrons but equally localized and concentrated in spikes, which are, because of the more difficult penetration, less homogeneously distributed through the material. Fast electrons (e) only produce one Frenkel defect each, at least if they do not possess too much kinetic energy, and these defects are randomly distributed. γ-rays occasionally cause ionization, thereby releasing a fast electron, which then in turn effects one displacement. The mean penetration is very large.

Figure 2-12: Irradiation damage caused by various particles in metals, Van Bueren, 1961.

2.3.2 Zirconium Alloys

In structural materials like Zircaloy, the overwhelming majority of defects are caused by neutrons, and the most important type of defect is the dislocation loop. Two types of loops predominate: <a> and <c> loops. The <a> loop lies on a prism plane and has a Burgers vector in the <a>-direction of the HCP lattice (see Figure 2-6**,** Figure 2-7 and, Figure 2-8). Table 2-1 lists some important characteristics. Both vacancy and interstitial loops exist, but more than half have vacancy character. They are very small (100 nm "black spots") and even in the transmission electron microscope (TEM) are difficult to analyze, Figure 2-13.

<a> loops form early in the irradiation and the number density reaches a saturation value at a fuel burnup less than 5 GWd/MT. The size of the loops increases with irradiation temperature, and the loops become unstable (start to disappear) at about 673K (400˚C). As will be discussed later they have a strong effect on mechanical properties.

Table 2-1: Radiation Damage, <a> loops in Zircaloy

Nature	vacancy(excess), interstitial
Size	8 –20 nm (80-200 Å)
Density	8 X 10^{14} m^{-2}
Saturation Fluence	1 X 10^{25} n m^{-2} (E>1 MeV)
Thermal stability	to about 400°C (673 K)
Effect	strength, ductility, growth

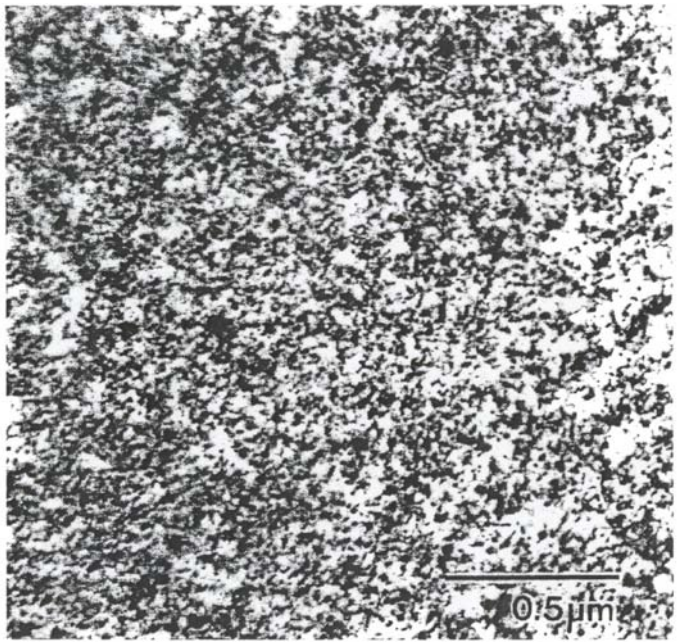

Figure 2-13: <a> type dislocation loops in neutron irradiated Zircaloy-2 (after post-irradiation annealing at 723 K for 1 hour).

The <c> type of loop lies on the basal plane and has its Burgers vector, or at least a strong component of it, in the c-direction of the HCP cell. As indicated in Table 2-2, unlike the <a> loop, it is strictly a vacancy-type loop, is relatively large (100 nm) and does not form until considerable irradiation effects have occurred. In Zircaloy <c> loops are first observed by TEM at a burnup of around 15 GWd/MT and increase in density the rest of the fuel lifetime. They are thermally stable to high temperature (>833K). <c> loops are thought to strongly influence irradiation growth and creep behavior, and probably do not affect mechanical properties. Figure 2-14 shows TEM images of a high density of <c> loops in highly irradiated Zircaloy. Such <c> loops do not appear to form in all zirconium alloys, particularly in those having additions of Nb or Nb and Fe, Shishov et al., 2002.

Table 2-2: Radiation Damage, <c> loops in Zircaloy

Nature	**Vacancy**
Size	> 100 nm (1000 Å)
Density	0.5 X 1014 m^{-2} (For Figure 2-14)
Incubation Fluence	3 X 10^{25} n m^{-2} (E>1 MeV)
Thermal	stable to >560°C (833 K) form at >200°C (475 K)
Effect	growth, creep ?

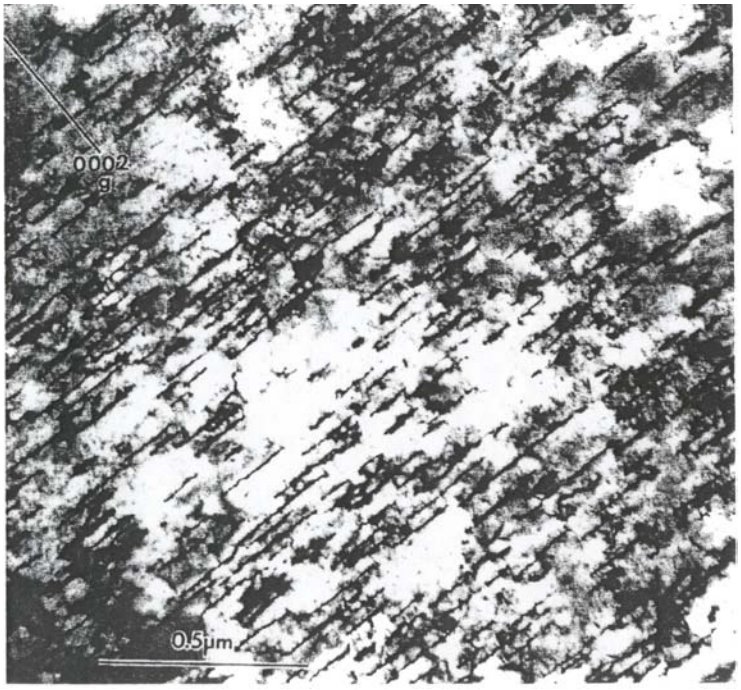

Figure 2-14: <c> type dislocations in Zircaloy-4 after a fluence of 12 x 10^{21} n/m^2 at 561 K.

As outlined in Table 2-1 and Table 2-2 the kinetics of formation of <a> and <c>-type loops differ. The density of <a> type dislocation builds up quickly and saturates at a fluence less than 1 x 10^{25} n/m^2, E >1 MeV, as illustrated in Figure 2-15. It appears that a fluence-incubation period exists before <c>-type loops begin to form at about 3 x 10^{25} n/m^2, E > 1 MeV for typical reactor temperatures, as illustrated in Figure 2-16.

For a straightforward review of the relation between irradiation-induced microstructure and Zircaloy properties see Adamson, 2000. More technical details and references can be found there.

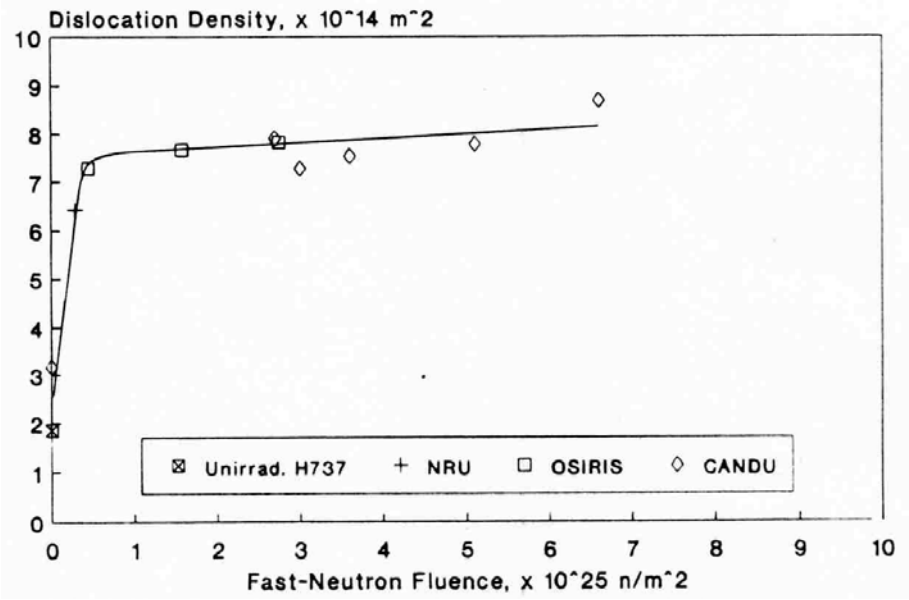

Figure 2-15: Variation of a-type dislocation loop density x 10^{14} m^{-2} as a function of fluence x 10^{25} $n{\cdot}m^{-2}$ in various reactors at 250-290°C (523-563K), Davies et al., 1994.

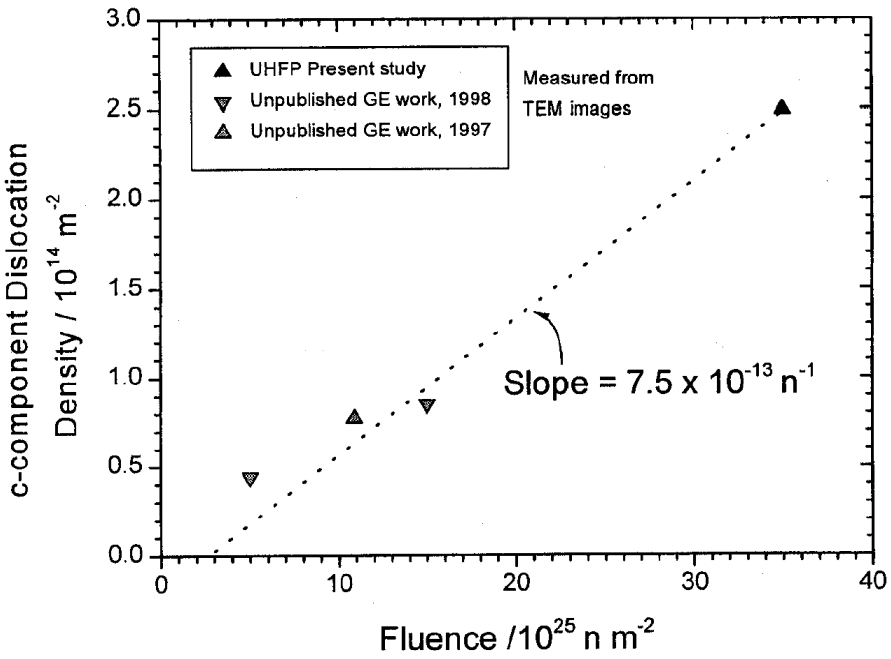

Figure 2-16: Variation of c-type dislocation density as a function of fluence for Zircaloy-2 irradiated at 290°C (563K), Mahmood et al., 2000.

2.4 IRRADIATION EFFECTS ON PRECIPITATES (SPPS)

Corrosion resistance in zirconium alloys is intimately related to the presence of second phase precipitates (SPPs) formed in the zirconium matrix by deliberate additions of alloying elements. The precipitates are usually incoherent crystalline intermetallic compounds, meaning that their physical structure is unrelated to the Zr matrix in which they are imbedded. In as-fabricated Zircaloy-4 the most common SPP is $Zr(Fe,Cr)_2$, while in Zircaloy-2 they are $Zr(Fe,Cr)_2$ and $Zr_2(Fe, Ni)$. For the ZrNb type alloys the most common is βNb (which is not an intermetallic) and for the ZrSnNbFe alloy types are $Zr(Nb,Fe)_2$ and βNb. Table 2-3 gives a more complete description, plus indicating some neutron irradiation effects.

At normal light water reactor temperatures (270-370°C (543-643K)) the SPPs change under irradiation in a combination of two ways – amorphization and dissolution.

Amorphization means that the original SPP crystalline structure is converted to an amorphous structure. Amorphization is a complex process, described in some detail by Griffiths et al., 1987, Yang,1989, Motta, 1997, Bajaj, et al., 2002, Taylor et al., 1999 etc. It occurs when an intermetallic compound accumulates enough irradiation-induced defects to cause it to thermodynamically favor an amorphous rather than a crystalline structure. The rate of amorphization depends on the relative rates of damage creation and damage annealing in the SPP; therefore important parameters are neutron flux, irradiation temperature and SPP chemistry. A critical temperature exists above which the annealing processes are fast enough to prevent the damage accumulation of defects needed for transformation. For typical reactor irradiations amorphization of both $Zr(FeCr)_2$ and $Zr_2(FeNi)$ occurs readily at temperatures near 100°C (373K) (although, and partly because, Fe is not released from the SPPs into the Zr matrix, to be discussed below). At typical LWR temperatures (300°C(573K)) and neutron flux $Zr(Fe,Cr)_2$ becomes amorphous but $Zr_2(FeNi)$ does not. Above about 330°C (603K) neither SPP becomes amorphous.

The amorphization process begins at the outside surface of the SPP and works its way inward with increasing fluence. This is illustrated in Figure 2-17, Yang et al., 1986, where the SPP on the left has an amorphous rim (dark area) and the one on the right, at higher fluence, is fully amorphous. There appears to be an incubation period prior to initiation of amorphization, with the incubation fluence decreasing with decreasing temperature in the range 270 -330 °C (543 -603K).

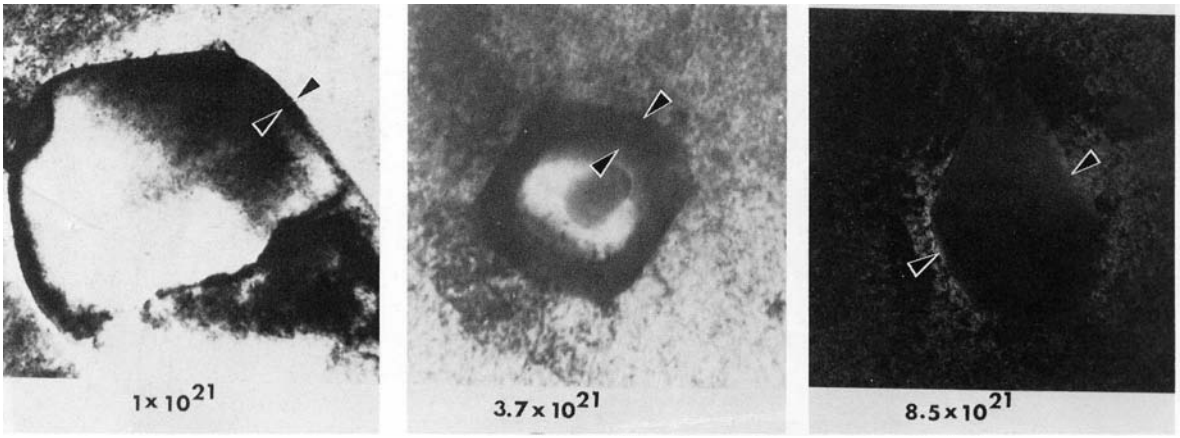

Figure 2-17: The fluence dependence of the amorphous transformation of $Zr(Fe,Cr)_2$ precipitate in RXA Zircaloy-4, neutron irradiated at 288°C(561K). The arrows indicate the width of the amorphous region. Yang et al., 1986.

Amorphization rate increases as temperature decreases, as neutron flux increases, and as SPP size decreases. Literature evaluation therefore needs to be compared to reactor and material conditions of specific interest.

The fluence required to produce complete amorphization depends on neutron flux, temperature and SPP size, but for typical $Zr(Fe,Cr)_2$ SPPs of initial size near 0.1 μm, the entire SPP is amorphous by end of bundle life burnups, <50 MWd/KgU ($1x10^{22}$ n/cm^2, E>1 MeV). Interestingly, under well controlled conditions of flux and temperature, the amorphization rate of $Zr(Fe,Cr)_2$ in Zircaloys can be used to estimate the neutron fluence using an equation F = RT where F is the fluence, T is the amorphous rim thickness and R is the experimentally determined amorphization rate. For irradiation temperature near 300°C (573K) in a BWR, the value of R is very approximately 10^{20} (n/cm^2, E > 1MeV)/nm, Motta & Lemaignan, 1992 and Bajaj, et al., 2002.

For the Zr-Nb type alloys neither the βNb or $Zr(Nb,Fe)_2$ SPPs become amorphous for irradiation temperature >330°C (603K). However, at 60°C (333K) $Zr(Nb,Fe)_2$ does become amorphous at high fluences.

SPP amorphization in itself does not appear to affect material behavior; however, dissolution of both amorphous and crystalline SPPs does influence corrosion, growth and mechanical properties, to be discussed later. At typical LWR operating temperatures, SPP dissolution occurs relentlessly until the SPP essentially disappears.

As SPPs dissolve, the zirconium matrix becomes enriched (well beyond the normal solubility limit) in the dissolving element. For instance in Zircaloy-2, Fe leaves both $Zr(Fe,Cr)_2$ and $Zr_2(Fe,Ni)$ SPPs as schematically illustrated in Figure 2-18**,** Mahmood et al., 2000. This process is given in more detail by Takagawa et al., 2004, Figure 2-19. Here it is seen that Fe rapidly diffuses from the amorphous rim into the matrix, while Cr diffusion is sluggish. At high fluence (~$1X10^{22}$ n/m^2, E > 1 MeV) complete amorphization and Fe-depletion has occurred, while the Cr level is still high. Only at very high fluence (~$1.5X10^{22}$ n/m^2, E > 1 MeV) is the Cr dispersed into the matrix, and the SPP essentially disappears.

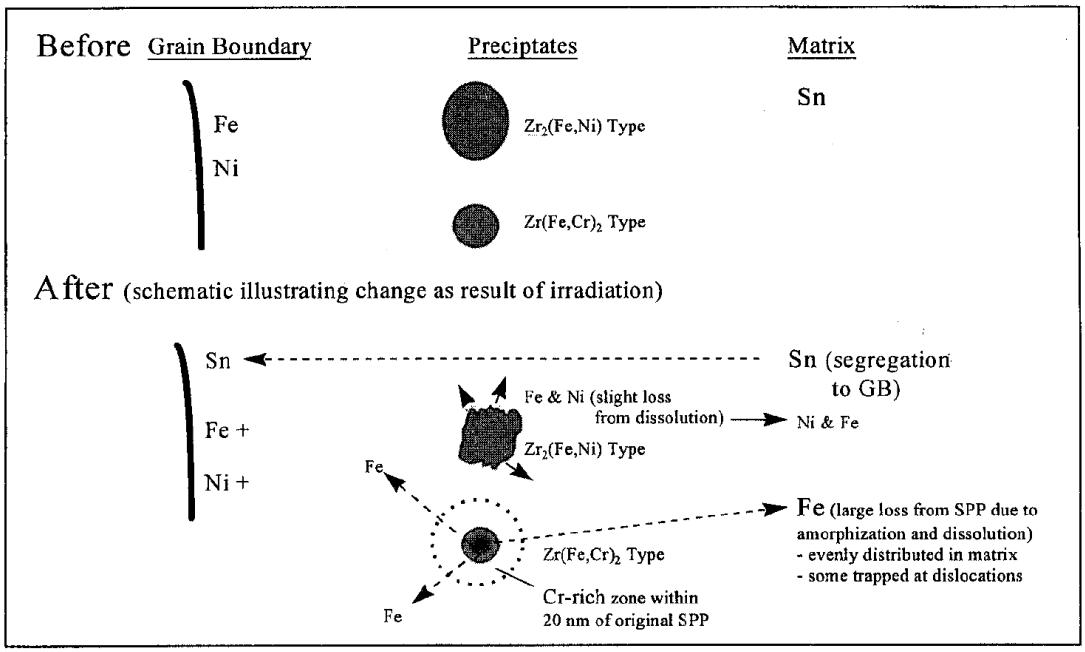

Figure 2-18: Schematic illustrating SPP dissolution and solute redistribution for small SPP Zircaloy-2 irradiated near 300°C, Mahmood, et al., 2000.

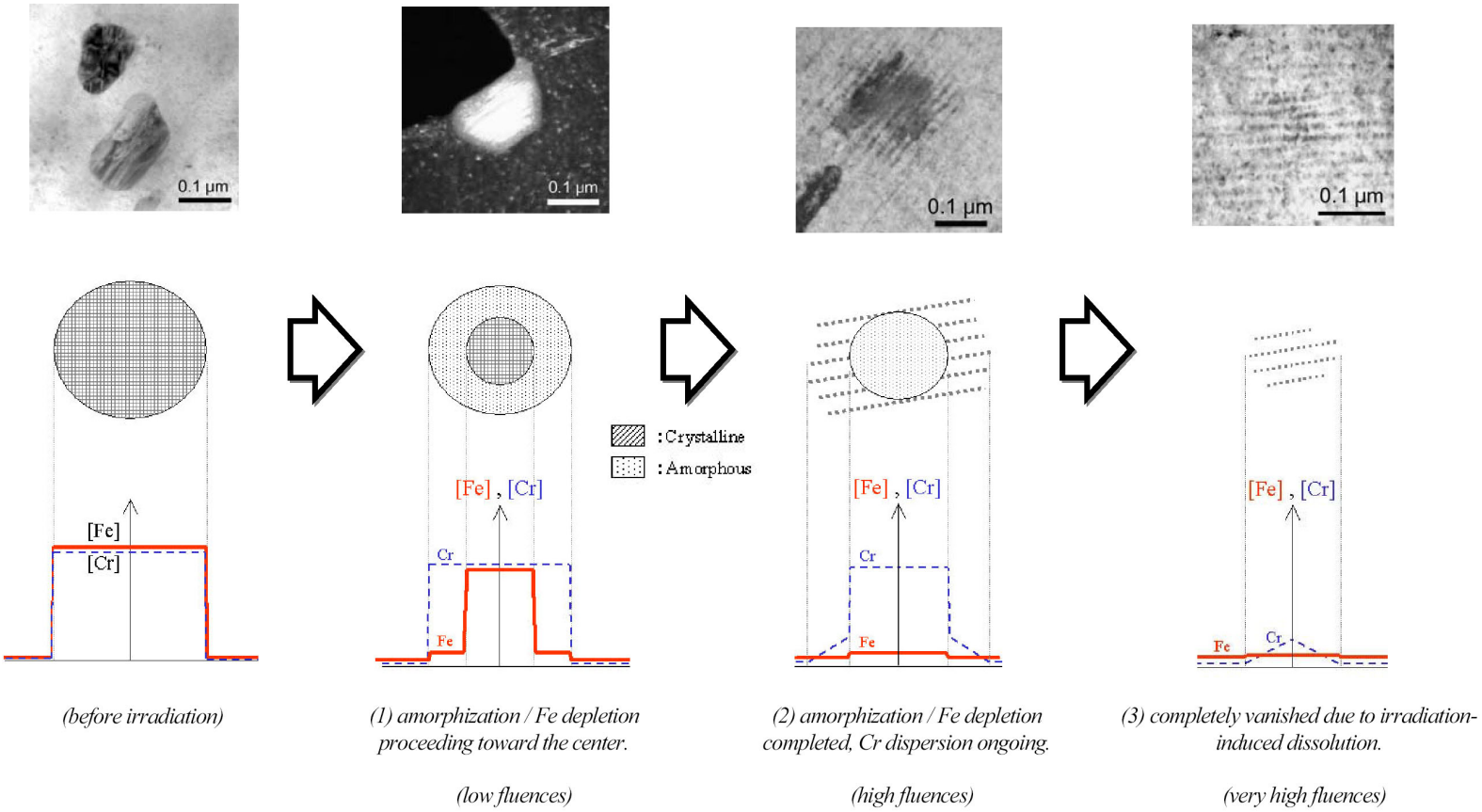

Figure 2-19: Evolution of a Zr-Fe-Cr particle under BWR irradiation. Upper figures: TEM micrographs; Middle diagrams: schematic illustration of amorphization; Bottom diagrams: schematic illustrations of the chemical compositions. Takagawa et al., 2004.

The rate of dissolution depends on the SPP size (higher rate for smaller sizes), and the extent of dissolution depends on size and fluence. It has been demonstrated in a BWR that small (<.04 μm) SPPs can completely dissolve at low to moderate burnups, Huang, et al., 1996. Also in a PWR, but at temperature near 290°C, SPPs with an average size of 0.2 μm were >80% dissolved at moderate burnup (1 x 10^{26} n/m^2, E > 1MeV), Garzarolli et al., 2002.

Modeling of the dissolution process gives insight into the alloying concentration of the matrix, Mahmood et al., 1997. Figure 2-20 illustrates the model for release of solute into the matrix for various size SPPs. For the small SPPs (1R, 2R, 3R) all the Fe is released by moderate burnup.

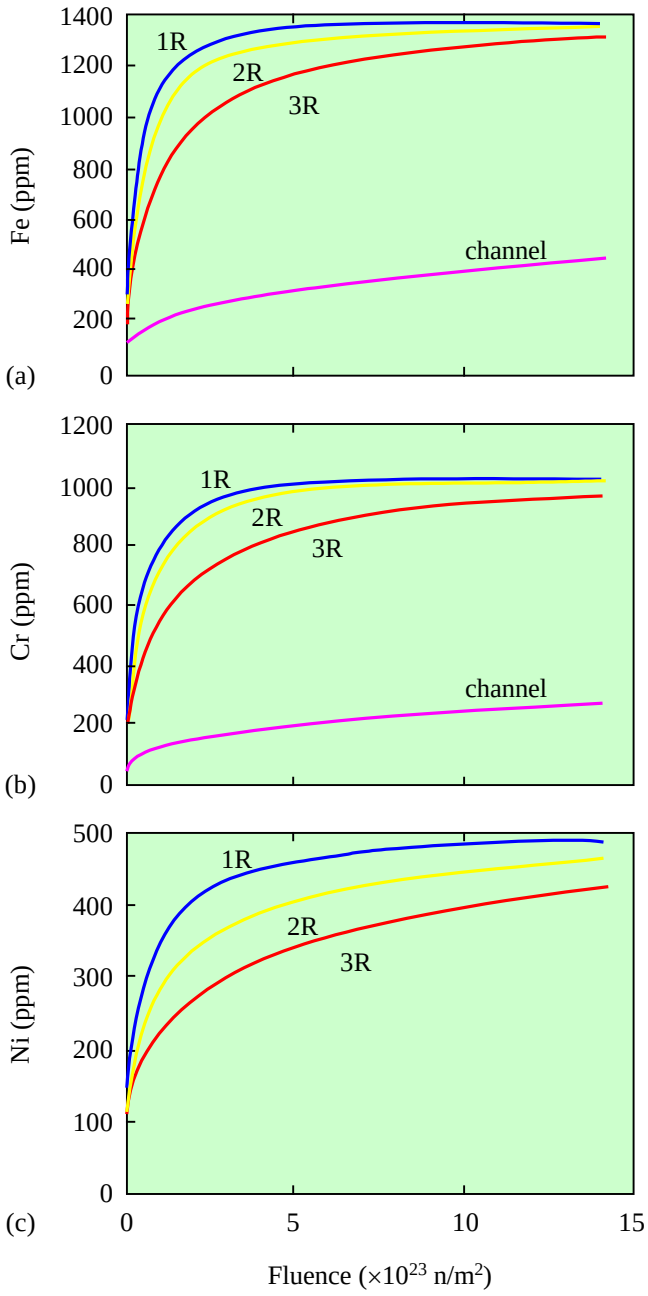

Figure 2-20: Modeling predictions for solute release to the matrix as a function of fluence for Zircaloy-2 (initial SPP size: 1R=.026 µm; 2R=.042 µm; 3R=.056 µm and Zircaloy-4 channel= 0.6 µm) irradiated near 300°C, modified figure according to Mahmood, et al., 1997.

For the channel material with very large (.6 µm) SPPs in the unirradiated state only a small amount of Fe would be released even at high burnups.

3 MECHANICAL PROPERTIES (RON ADAMSON)

3.1 OVERVIEW

By ”mechanical properties” we essentially mean strength and ductility. Strength is expressed in terms of hardness, tensile strength, burst strength, fatigue strength, etc. Ductility is likewise expressed in terms of strain-to-failure or strain-to-some limit for the various loading conditions. Fracture toughness is a combination of strength and ductility which describes the stress required to propagate a specific crack geometry under specific loading conditions. In this section we discuss various mechanical properties as affected by reactor neutron irradiation. In addition, we describe mechanisms and parameters which are related to mechanical properties and which affect reactor component behavior. This section deals primarily with properties which can be determined by out-of-reactor (or post-irradiation) testing. For instance tensile properties (strength and ductility) of interest for in-reactor performance are mainly dependent on fluence and independent of flux. However, if the rate at which strain is applied becomes very low ($<10^{-6}$ sec^{-1}), the mechanism of deformation changes, and flux becomes an important variable, Azzarto et al., 1969. That phenomenon is dealt with more as creep, in the section on dimensional stability.

As described in Section 2, neutron irradiation dramatically alters the microstructure of zirconium alloys. Of importance for mechanical properties are creation of <a> dislocation loops, and to a lesser extent, dissolution of precipitates (SPPs). Irradiation increases strength and hardness, and decreases ductility. The effect on fatigue life (or strength) is less clear and depends on testing technique, but generally appears to be small, with some reduction of fatigue life in the low cycle region. Fracture toughness is clearly reduced by irradiation in Zr 2.5 Nb, and there are indications of a smaller reduction in Zircaloys. The combination of irradiation and hydride effects is important; for uniformly distributed hydrides the observed reduction in ductility is mainly an irradiation, rather than a hydride effect; however concentrations of hydrides (rims, blisters) can overwhelm irradiation effects. Details are given in the following sub-sections.

3.2 EFFECTS ON STRENGTH

As outlined in Section 2.3.2, irradiation produces damage in the form of small dislocation loops (<a> component loops) which harden the material. The result is an increase in strength and decrease in ductility.

At reactor start-up, the tensile properties are the unirradiated properties reported by the fuel supplier. Mechanical properties begin changing immediately upon startup, and by an exposure of 5 MWd/KgU or a fluence of about $1x10^{25}$ n/m^2 (E>1MeV) strength and ductility reach fluence-saturated values. Figure 3-1 illustrates this point for Zircaloy-4 irradiated and tested at 588K (315°C) [after Morize et al., 1987]. Note also that the ultimate tensile strengths (UTS) of cold worked stress relieved (CWSR) and recrystallized (RX) materials become similar at low exposures. This is a general trend which depends on the balance of hardening by pre-existing dislocations (cold work) and irradiation produced defects. It is known that the irradiation growth rate of cold worked material is initially much higher than for recrystallized material (see Section 4), indicating that some of the irradiation-produced point defects are absorbed by existing dislocations rather than forming <a> loops.

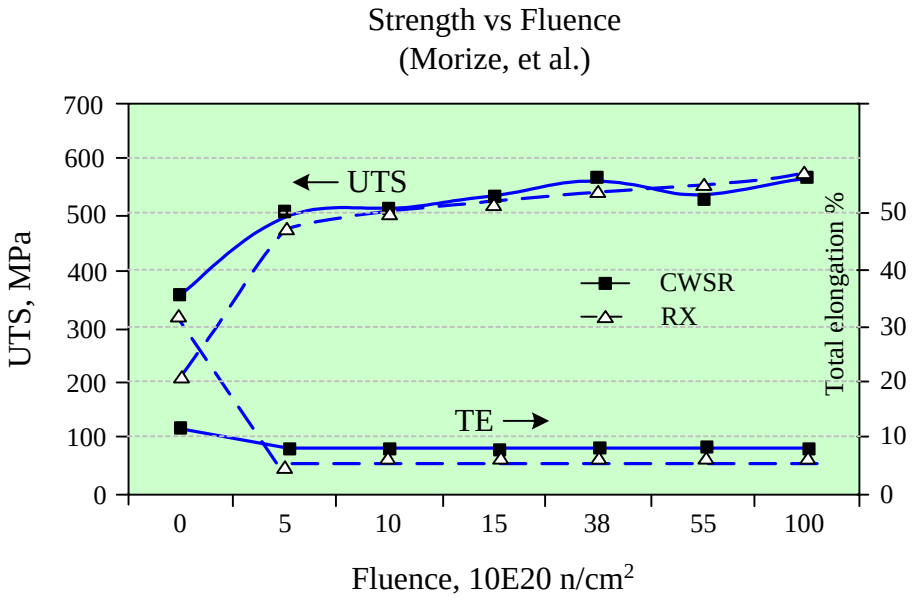

Figure 3-1: Effect of neutron fluence on strength and ductility of recrystallized (RX) or cold-worked (CWSR) Zircaloy, modified figure according to Morize et al., 1987.

Fuel cladding requires sufficient strength to prevent inward plastic deformation of the cladding at beginning-of-service conditions. PWR strength must be higher than for BWRs due to the higher water pressure needed to suppress boiling; therefore, PWR Zircaloy cladding has traditionally been in the cold work stress relieved (SRA) condition. The discussion above points out that the difference in strength between SRA and RXA materials is short-lived in reactor.

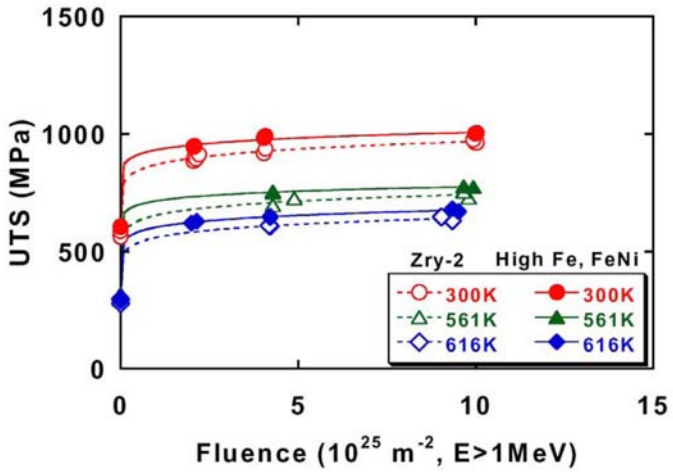

Figure 3-2: Ultimate tensile stress of Zircaloy-2, High Fe and High FeNi,. Ishimoto et al., 2003.

For the RXA Zircaloy-types, Figure 3-2 confirms saturation out to high fluence. For Zr1Nb, the saturation of strength (and ductility) may occur at even lower fluence. Figure 3-3, Griger, 2004, indicates that saturation occurs near $3X10^{24}$ n/m^2 (energy is not given but probably is >1 MeV). For the Nb-containing alloys true saturation is shown by the high fluence data in Figure 3-4, Tsukuda et al., 2003.

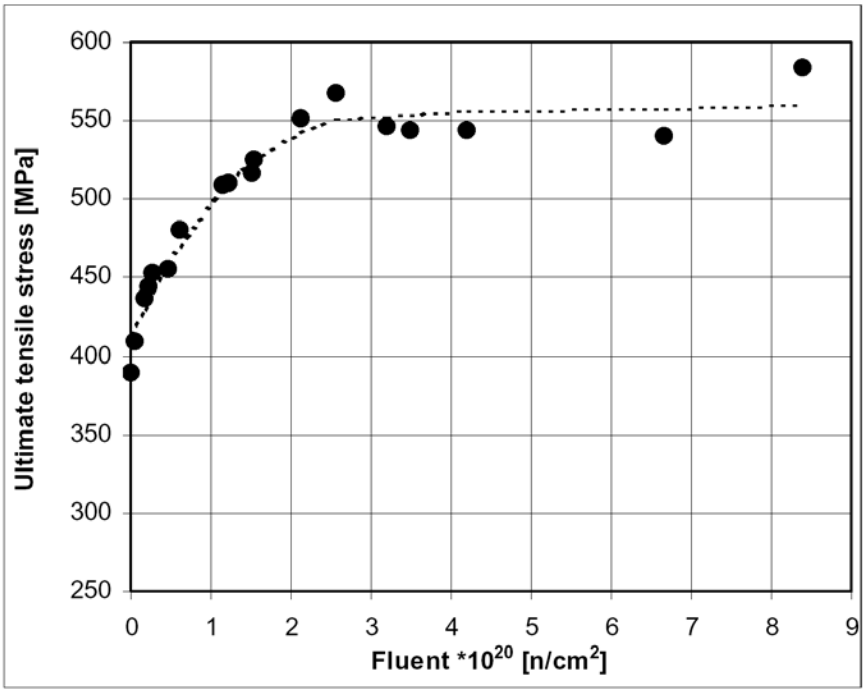

Figure 3-3: Ultimate tensile stress of Zr1Nb cladding as a function of fluence, Griger, 2004.

4 DIMENSIONAL STABILITY (RON ADAMSON)

4.1 INTRODUCTION

One of the most unique aspects of material behavior in a nuclear power plant is the effect of radiation (mainly neutrons) on the dimensional stability of the reactor components. In fast breeder reactors the Fe and Ni-based alloys creep and swell, that is, they change dimensions in response to a stress and change their volume in response to radiation damage. In light water reactors, zirconium alloy structural components creep, do not swell, but do change their dimensions through the approximately constant volume process called irradiation growth. Radiation effects are not unexpected since during the lifetime of a typical component every atom is displaced from its normal lattice position at least 20 times. With the possible exception of elastic properties like Young's Modulus, the properties needed for reliable fuel assembly performance are affected by irradiation. A summary of such effects is given by Adamson, 2000.

Practical effects of dimensional instabilities are well known and it is a rare technical conference in the reactor performance field that does not include discussions on the topic. Because of the difference in pressure inside and outside the fuel rod, cladding creeps down on the fuel early in life, and then creeps out again later in life as the fuel begins to swell. A major issue is to have creep strength sufficient to resist outward movement of the cladding if fission gas pressure becomes high at high burnups. *PWR* guide tubes can creep downward or laterally due to forces imposed by fuel assembly hold down forces or cross flow hydraulic forces – both leading to assembly bow which can interfere with smooth control rod motion. *BWR* channels can creep out or budge in response to differential water pressures across the channel wall, again leading toward control blade interference. Fuel rods, water rods or boxes, guide tubes, and tie rods can lengthen, possibly leading to bowing problems. (For calibration, a recrystallized (RX or *RXA*) Zircaloy water rod or guide tube could lengthen due to irradiation growth more than 2 cm. during service; a cold worked/stress relieved (*SRA*) component could lengthen more than 6 cm.) Even RX spacer/grids could widen enough due to irradiation growth (if texture or heat treatment was not optimized) to cause uncomfortable interference with the channel.

In addition, corrosion leading to hydrogen absorption in Zircaloy can contribute to component dimensional instability due, at least in part, to the fact that the volume of zirconium hydride is about 16% larger than zirconium.

The above discussion leads to the concept that understanding the mechanisms of dimensional instability in the aggressive environment of the nuclear core is important for more than just academic reasons. Reliability of materials and structure performance can depend on such understanding.

A comprehensive review of dimensional stability has been given in the ZIRAT 7 Special Topical Report; Adamson & Rudling, 2002. The sources of dimensional changes of reactor components (in addition to changes caused by conventional thermal expansion and contraction) are: irradiation growth, irradiation creep, thermal creep, stress relaxation (which is a combination of thermal and irradiation creep), and hydrogen and hydride formation.

Irradiation effects are primarily related to the flow of irradiation-produced point defects to sinks such as grain boundaries, deformation-produced dislocations, irradiation-produced dislocation loops, and alloying and impurity element complexes. In zirconium alloys, crystallographic and diffusional anisotropy are key elements in producing dimensional changes.

In the past, hydrogen effects have been considered to be additive to and independent of irradiation; however, recent data have brought this assumption into question. It is certain that corrosion-produced hydrogen does cause significant dimensional changes simply due to the 16-17% difference in density between zirconium hydride and zirconium. A length change of on the order of 0.25% can be induced by 1000 ppm hydrogen in an unirradiated material. Whether or not the presence of hydrides contributes to the mechanisms of irradiation creep and growth is yet to be determined.

Fuel rod diametral changes are caused by stress dependent creep processes. Fuel rod length changes are caused by several phenomena:

- Stress free axial elongation due to irradiation growth.
- Anisotropic creep (before pellet/cladding contact) due to external reactor system pressure. Because of the tubing texture, axial elongation generally results from creep down of the cladding diameter; however for heavily cold worked material, it has been reported that some shrinkage may occur. In a non-textured material such as stainless steel, creep down of the cladding would only result in an increase in cladding thickness, with no change in length.
- Creep due to pellet-cladding mechanical interaction (*PCMI*) after hard contact between the cladding and fuel. This occurs in mid-life, depending on the cladding creep properties and the stability of the fuel.
- Hydriding of the cladding due to corrosion.

Bow of a component such as a *BWR* channel or *PWR* control rod assembly can occur if one side of the component changes length more than the other side. Such differential length changes occur due to differential stress and creep, to relaxation of differential residual stresses, or to differential growth due to differences in flux-induced fluence, texture, material cold work, and hydrogen content (and, although not usually present, differences in temperature or alloying content). This is described more in the ZIRAT 10 Special Topics Report on Structural Behaviour of Fuel and Fuel Components, 2005.

This section discusses the effect of irradiation on dimensional stability.

4.2 IRRADIATION GROWTH

4.2.1 Basics

Irradiation growth is a change in the dimensions of a zirconium alloy reactor component even though the applied stress is nominally zero. It is approximately a constant volume process, so if there is, for example, an increase in the length of a component, the width and/or thickness must decrease to maintain constant volume. Understanding of the detailed mechanism is still evolving; however a clear correlation of growth to microstructure evolution exists, and many empirical observations have revealed key mechanistic aspects. The inherent anisotropy of the Zr crystallographic structure plays a strong role in the mechanism, as materials with isotropic crystallographic structure (like stainless steel, copper, Inconel, etc.) do not undergo irradiation growth. It is not to be confused with irradiation swelling, which does conserve volume and does not occur in zirconium alloys under normal reactor operating conditions.

Irradiation growth is strongly affected by fluence, cold work, texture, irradiation temperature, and material chemistry (alloying and impurity elements), as will be described in later sections. Figure 4-1 gives schematic growth curves illustrating several points. Note that L-textured material grows, while T-textured material shrinks; when taken with the third direction (N) in a component, this behaviour results in approximately constant volume. The long direction (L) of a component is the most important; for instance the length of a fuel rod, channel box or guide tube. Note that cold worked (CW) material grows at a high and almost linear rate, while recrystallized (RXA) material grows in a 3-stage process, with the final high rate being called “breakaway” growth. The various stages can be directly related to the irradiation-produced microstructure described in Section 2.3. For RXA Zircaloy, at low fluences where only <a> component loops exist, growth is small (~0.1%) and saturates. When <c> component loops begin to appear the growth rate increases and becomes nearly linear with fluence in the range 6-10 x 10^{25} n/m^2, E > 1 MeV. For L-texture material growth can reach 1% at 20 x 10^{25} n/m^2. In initially cold worked (CW) or cold worked.

5 IMPACT OF IRRADIATION ON HYDROGEN SOLUBILITY IN ZR (BRIAN COX)

The solubility of hydrogen (*TSS*) in zirconium alloys varies significantly from alloy to alloy, especially in Zr-Nb alloys where concentrations of β-Zr may be significant and *TSS* in β-Zr is much higher than in α-Zr, Figure 5-1, Cox & Rudling, 2000. It has been known since early studies of tritium migration in zirconium alloys, Roy, 1965 that hydrogen could be trapped at dislocations in these alloys. Specimens in these tests had tritium absorbed in them at 700°C; they were then rapidly quenched to room temperature to give random metastable solid solution of T_2 in α-Zr. The specimens were then strained to generate slip bands, Figure 5-2(a) and autoradiographed to locate the tritium, Figure 5-2(b). The tritium was found to be concentrated along the slip bands (i.e. trapped at the dislocations). Unfortunately the two micrographs are not of the same area. This work clearly showed that H could be trapped at dislocations in unirradiated Zr. However, no estimates of the quantity of trapped hydrogen can be obtained from these results, since tritium autoradiography is very sensitive to small quantities of T, and is not easily calibrated. No anneal and quench tests were done to establish the temperature at which the H/T was released from the dislocations.

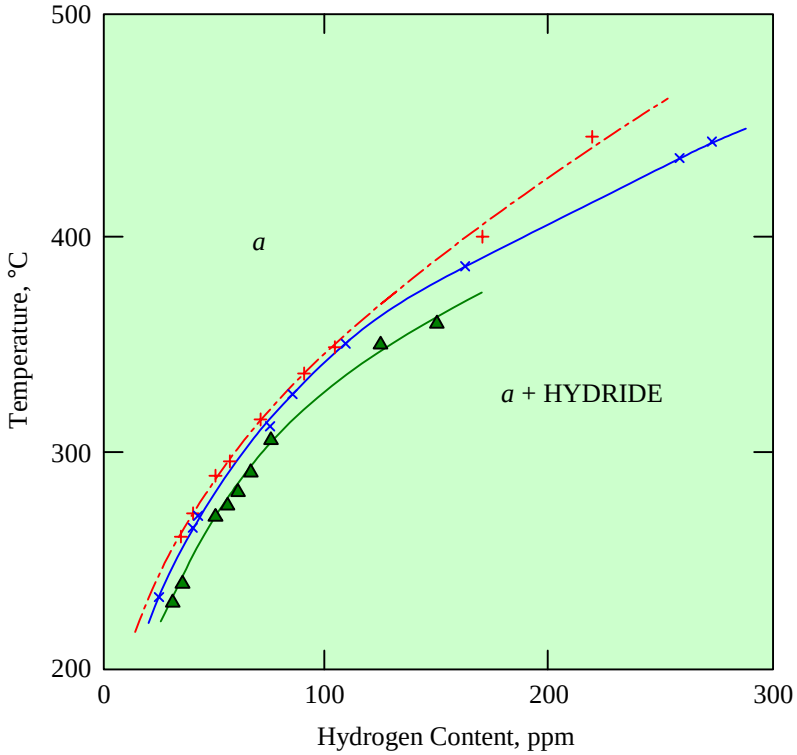

a)

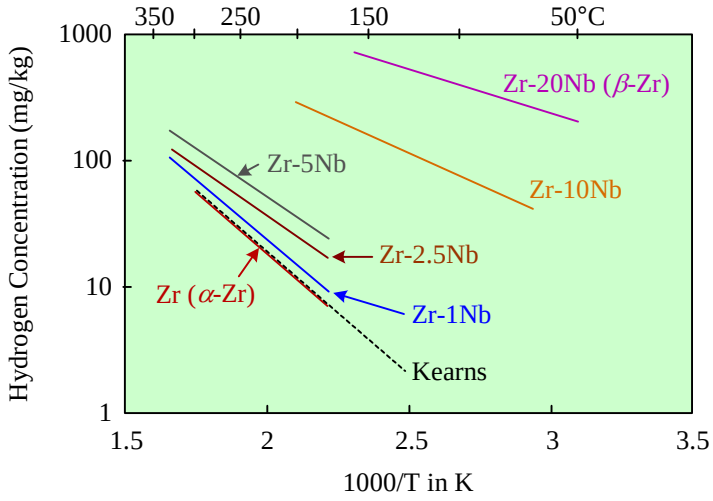

b)

Figure 5-1: H solubility differences between Zr-alloys, (a) (▲)Zry-2, (**X**) Zry-4, (+) Zr2.5Nb; (b) TSS_d lines for hydrogen in Zr-Nb specimens with different Nb concentrations annealed at 1123 K for 1h. The lines for α-Zr and annealed Zr-20Nb (β-Zr) as well as the Kearn's line for unalloyed Zr are included for comparison, Cox and Rudling, 2000

a)

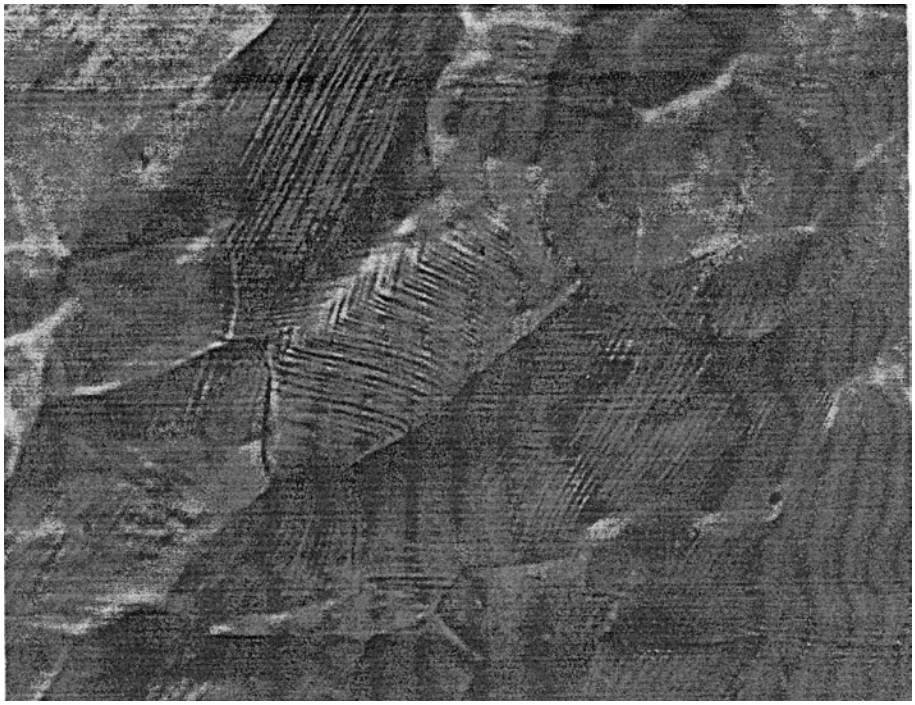

b)

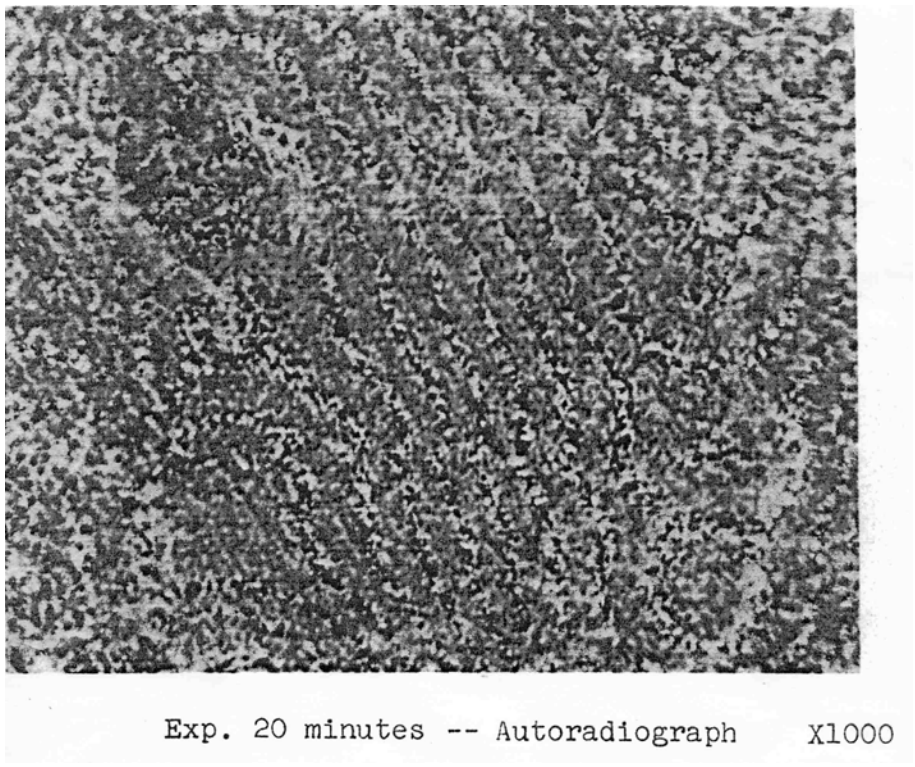

Figure 5-2: Tensile specimen (containing 240 ppm T_2) heated at 700°C and water quenched. Deformed at RT by ~8%. (a) Micrograph showing slip steps on the surface, (b) Autoradiograph of unmounted specimen, Roy, 1965.

6 IMPACT OF IRRADIATION ON CORROSION (BRIAN COX)

6.1 IN THE METAL

Fast neutron irradiation displaces atoms from their lattice sites creating, initially, clusters of defects, which appear as “black spots” in *TEM* studies. These develop into dislocation loops that interact with the pre-existing forest dislocations and affect the mechanical properties. This has little or no effect on corrosion, however, in alloys containing Fe in the form intermetallic particles the fast neutrons displace Fe atoms from the *SPPs* into a metastable solution in the Zr matrix. This results in a progressive degradation of the oxidation resistance of the alloy in post irradiation tests, Figure 6-1, Cheng et al., 1994. Amorphisation of *SPPs* may also occur, but only the physical displacement of the Fe atoms affects the corrosion rate. In Zr-Nb alloys irradiation enhanced decomposition of the β-Zr phase will reduce the corrosion rate in-reactor, since β-Zr corrodes faster than α-Zr. This enhanced decomposition can be achieved by the enhanced metallic diffusion that can be caused by any radiation flux capable of producing Frenkel Pairs, physical recoil of atoms out of the β-Zr phase is not required. Thus, the effect is seen with high energy electrons and does not require fast neutron recoils, Figure 6-2(a), Woo et al., 2000. No effect is seen for Zircaloy, Figure 6-2(b).

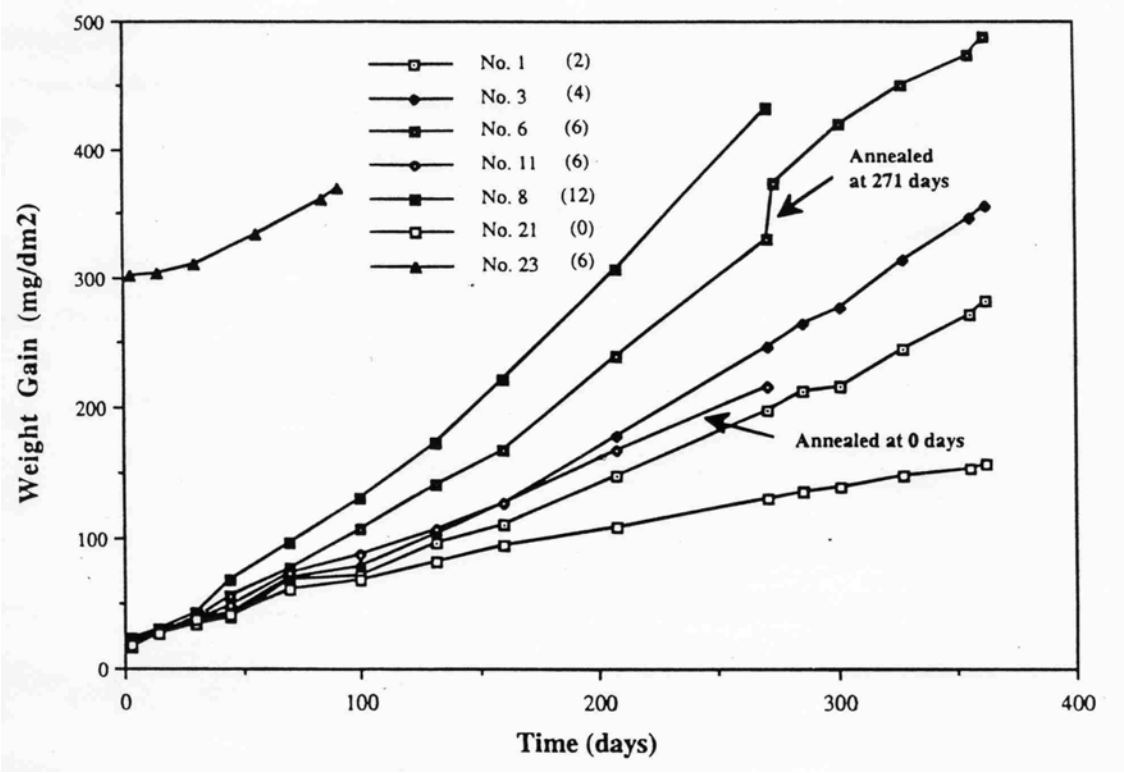

Figure 6-1: Corrosion of Zircaloy-2 in 400°C (673 K) steam. BWR water rod materials irradiated at 288°C (561 K). Fluences are given in parenthesis, 10^{25} n/m^2 (E>1 MeV), Cheng et al., 1994.

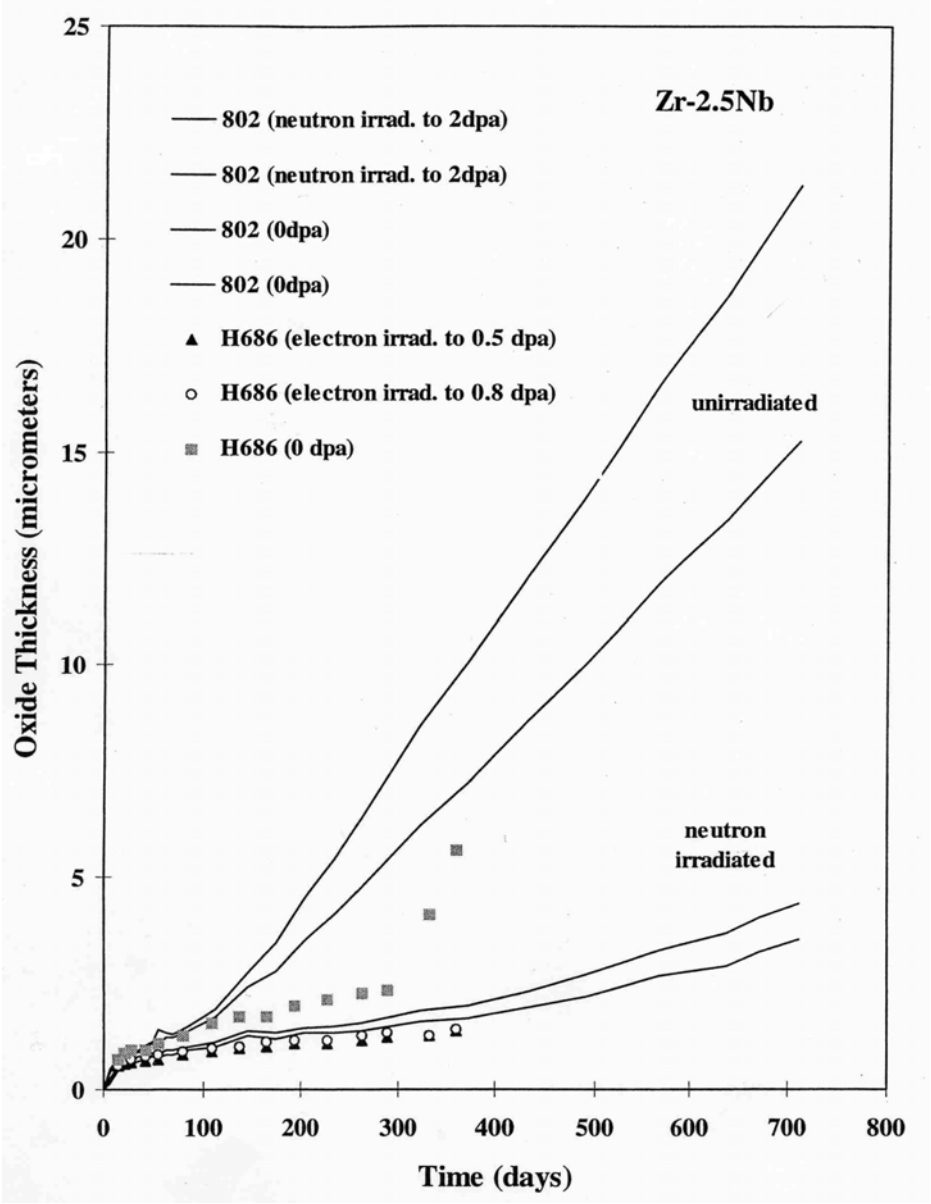

Figure 6-2(a): Comparison of the corrosion response in 300°C moist air of Zr-2.5Nb (H686) electron-irradiated at ≈450°C with neutron-irradiated Zr-2.5Nb (#802) material. #802 is standard cold-worked Zr-2.5Nb CANDU pressure tube that has been removed from Pickering Nuclear Generation Station. The solid curves are data from two samples each of unirradiated and neutron-irradiated Zr-2.5Nb (#802) material, Woo et al., 2000.

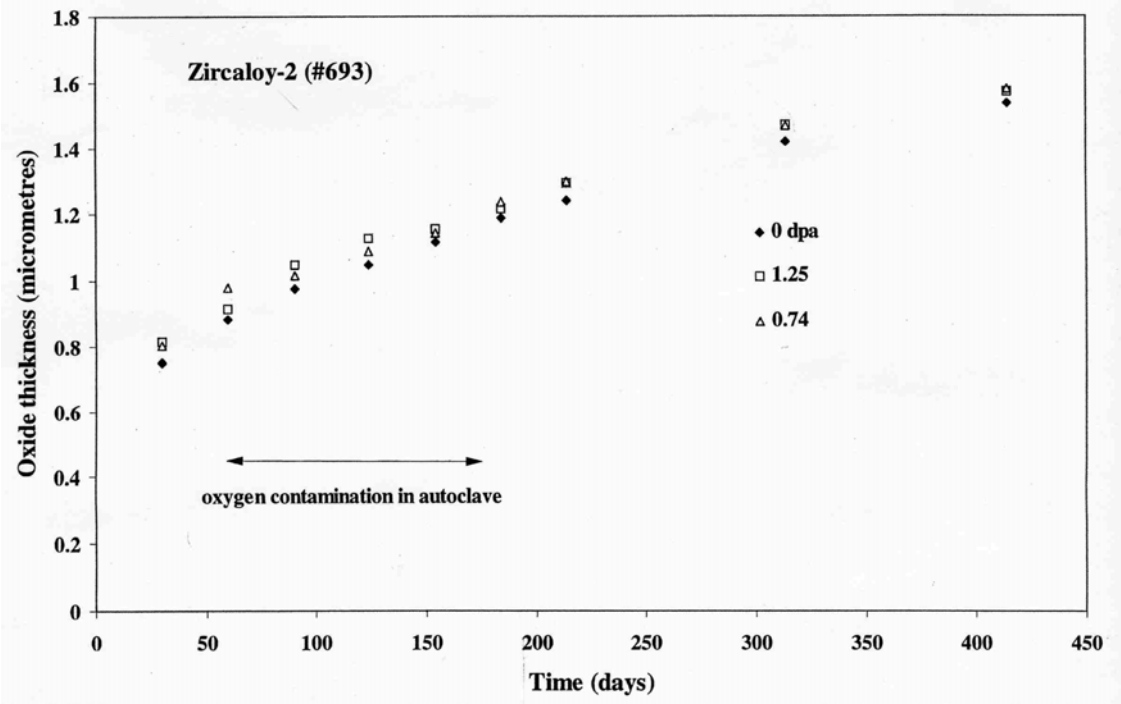

Figure 6-2(b) Corrosion response in 300°C D_2O of electron-irradiated (at low temperature) Zircaloy pressure tube material, #693, showing no difference between electron-irradiated and unirradiated, Woo et al., 2000.

6.2 IN THE OXIDE

Fast neutron irradiation will also displace atoms from their lattice sites in the protective oxide film, and so it was expected that oxygen diffusion controlled growth of the surface oxide would be accelerated, IAEA-TECDOC-996, 1998. However, no evidence for point defect clusters or dislocation loops have been found in oxide films grown under either proton, Spitznagel et al., 1973 or fast neutron bombardment, Woo et al., 2003. Apart from twinning of the ZrO_2 crystallites, thought to be the result of the tetragonal to monoclinic phase change, only nanopores which are probably a result of He production from the $^{16}O(n,\alpha)^{13}C$ reaction are seen, Figure 6-3.

Electron and gamma radiation both in-reactor and in laboratory tests cause enhanced electron conductivity in the oxide film, Figure 6-4, and this will lead to enhanced oxidation rates whenever the electronic conductivity of the oxide film is the rate determining step. This has been shown to be the case in most oxidation environments, except water at 300-350°C where the necessary measurements are almost impossible to make because of interference from poor reversibility of reactions in the aqueous phase for electron currents, Cox, 2005. If electron and gamma energies are high enough these radiations can also create Frenkel Pairs. Displacement energies are lower in the metal than in the oxide, so phenomena such as amorphisation of intermetallics, and enhanced diffusion induced decomposition of β-Zr in Zr-2.5%Nb can occur, but no enhanced diffusion in the oxide film is observed, Howe et al., 1994.

7 WRAP-UP

In this report, the effects of irradiation have been examined in several areas which directly or indirectly affect zirconium alloy component performance in the reactor core. Much knowledge has been gained through experiments and experience since the development, in the 1950's, of zirconium as a reactor material. We have reviewed in detail the current state-of-knowledge of the effects of irradiation on microstructure, mechanical properties, dimensional stability and corrosion. Perhaps astoundingly after so many years of experience but understandably when the increase in imposed reactor duty is considered, there are still areas that need additional work. The following cannot be claimed to be complete, but is certainly a guide for on-going and future study:

7.1 MICROSTRUCTURE AND MICROCHEMISTRY (ADDITIONAL UNDERSTANDING NEEDED)

- Factors which affect formation of <c> component dislocations.
- Details of second phase precipitate (SPP) dissolution.
- Chemical and fabrication detail, which could lead to dissolution-resistant SPPs.
- Details of the distribution of "solute" elements after and during SPP dissolution due to irradiation and due to fabrication variables.
- Reprecipitation of "solutes" and impurities at medium and high burnups.
- Effects of the evolving microchemistries during reactor service on details of the anisotropy and magnitude of "solute" diffusion.
- Interactions between irradiation-induced micro-structure and –chemistry and hydrogen solubility and mobility.

7.2 MECHANICAL PROPERTIES (ADDITIONAL UNDERSTANDING NEEDED)

- Effects of hydride distribution on failure strain.
- Development of a data base or bases that are relevant to specific issues, such as failure during reactivity insertion accidents.
- Fracture toughness at high burnup and for various hydride distributions, particularly for those components that are too thin for the application of standard linear elastic fracture mechanics.
- Detailed understanding of the mechanisms of irradiated material deformation.
- Refinement of the interaction between chemistry and mechanical aspects on pellet-cladding-interaction (PC)) failures.
- The exact role of hydrogen and hydrides on cladding axial long-split phenomena.

7.3 DIMENSIONAL STABILITY (ADDITIONAL UNDERSTANDING NEEDED)

- High burnup effects on the "constant volume" irradiation growth assumption, and on the reliability of the $g = g'(1-f_x)$ relationship for growth.
- Interactions or synergisms which exist between the irradiation growth/creep mechanisms and the presence of hydrogen and hydrides.
- Specific fundamental reasons for the difference in growth behavior of the various Zr1Nb alloys. This may include the effects of microchemistry variations.
- Detailed mapping of irradiation growth/creep behavior as a function of temperature, for BWR/PWRs between 270-380°C (543-653K).
- Resolution of the effects of reactor-formed oxides on growth/creep behavior of thin-walled core components.
- Detailed understanding of the reasons for the marked reduction of irradiation growth of Zr-Nb and Zr-Sn-Nb-Fe alloys compared to standard Zircaloys

7.4 CORROSION

Current views of the effects of irradiation on corrosion have been described according to their effects, respectively, on the metal; the oxide ; the reactor water; and the overall in-reactor effect. In the metal the primary impact of irradiation results from the displacement of Fe atoms from their normal lattice sites to produce a meta-stable solution in the Zr matrix. This has the effect of decreasing the corrosion resistance of the alloy, even in post-irradiation autoclave tests. In the oxide film, although displacement of atoms by fast neutrons must be occurring, there is no evidence either in oxide films or in zirconia inert-matrix fuel for point defect clusters or dislocations. The primary effect of irradiation seems to be to reduce the electrical resistivity of the oxide, thus increasing the corrosion rate by whatever factor the electronic conduction is more difficult than the ionic conduction. In the reactor water, although there will be much radiolysis in BWR water, there is no evidence for any direct effect of radiolytic species on a rate-controlling surface reaction. the primary effects of water radiolysis are two-fold: an increase in galvanic potential differences between different components of the reactor core ; and the possible local dissolution of the oxide crystallite boundaries by hydrogen peroxide. The overall effect in BWRs is to generate "Shadow" or "Nodular" corrosion, both of which are driven by galvanic cells between dissimilar metals. In the case of nodular corrosion the SPP is the dissimilar metal. The high H overpressures in PWRs eliminate galvanic effects due to dissimilar metals.

7.5 H SOLUBILITY

There are small differences in the H solubility in all Zr alloys and between different metallurgical conditions in the same alloy. These differences only become large for Zr-Nb alloys where the beta-Zr phase has a high H solubility. That hydrogen could be trapped at dislocations in Zr alloys has been known for a long time. It came as no surprise, therefore, that irradiation induced dislocation loops could increase the trapping of H, and thereby increase the TSS. That in highly irradiated materials, containing c-type dislocation loops, the effect could be much larger did come as a surprise. There still remain a number of questions about the mechanism of these effects that need resolving, including their potential effects on the high temperature embrittlement of Zr alloys. It is to be hoped that these questions will be answered by future experimental work.

Very much is known about the behavior of zirconium alloys as influenced by irradiation. This report documents much of this information. As more data and insights are gained, they will be documented in future ZIRAT Annual Reports.

8 REFERENCES

Adamson R. B., "*Irradiation Growth of Zircaloy", Zirconium in the Nuclear Industry; Third Conference,* ASTM STP 633, pp. 326, ASTM, 1977.

Adamson R. B., Tucker R. P. and Fidleris V., "*High-Temperature Irradiation Growth in Zircaloy*", Zirconium in the Nuclear Industry, 5th Conference, ASTM STP 754, D. G. Franklin, Ed., American Society for Testing and Materials, 208-234, 1982.

Adamson R. B. and Bell W. L., "*Effects of Neutron Irradiation and Oxygen Content on the Microstructure and Mechanical Properties of Zircaloy*", Microstructure and Mechanical Behavior of Materials, Proceedings: Int'l Symposiums, Xian, China, Oct. 1985, EMAS, Warley, UK, 237-246, 1986.

Adamson, R. B., Wisner, S. B., Tucker, R. P. and Rand. R. A., "*Failure Strain for Irradiated Zircaloy Based on Subsized Specimen Testing and Analysis*", The Use of Small-Scale Specimens for Testing Irradiated Material, ASTM STP 888, W. R. Corwin and G. E. Lucas, Eds., American Society for Testing and Materials, Philadelphia, 171-185, 1986.

Adamson R. B., "*Effects of Neutron Irradiation on Microstructure and Properties of Zircaloy*", Zirconium in the Nuclear Industry; Twelfth International Symposium, ASTM STP 1354, ASTM, pp. 15-31, West Conshohocken, PA, 2000.

Adamson, R. B. Private communication, 2001.

Adamson R. B. and Rudling P., "*Mechanical Properties of Zirconium Alloys*", ZIRAT-6 Special Topical Report, 2001.

Adamson R. B. and Rudling P., "*Dimension Stability of Zirconium Alloys*", ZIRAT-7 Special Topical Report, 2002.

Adamson R. B., Cox B., Garzarolli F., Strasser A., Rudling P. and Wikmark G., "*Corrosion of Zirconium Alloys*", ZIRAT-7 Special Topical Report, Dec., 2002.

Adamson R. B., Cox B., Garzarolli F., Strasser A., Rudling P. and Wikmark G., "*ZIRAT 8 Special Topics Report: High Burnup Fuel Issues*", 2003.

Alexander W. K., Fidleris V. and Holt R. A., "*Zry-2 pressure tube elongation at the Hanford N Reactor*", ASTM Spec. Techn. Publ. 633), pp. 344-, 1977.

Armas A. F. and Alvarez-Armas I., "*Cyclic Behavior or Zircaloy-4 at Elevated Temperatures*", Zirconium in the Nuclear Industry: Seventh Int'l Symposium, ASTM STP 939, R. B. Adamson and L. F. P. Van Swam, Eds., Am. Soc. for Testing and Materials, Philadelphia, 617-630, 1987.

Azzarto F. J., Baldwin E. E., Wiesinger F. W. and Lewis D. M., "*Unirradiated, In-Pile and Post-Irradiation Low Strain Rate Tensile Properties of Zircaloy-4*", Journal of Nuclear Materials, Vol. 30, pp. 208-218, 1969.

Bajaj R., Kammenzind B. F., and Farkas D. M., "*Effects of Neutron Irradiation on the Microstructure of Alpha-Annealed Zircaloy-4*", Zirconium in the Nuclear Industry: 13th International Symposium, ASTM STP 1423, G. D. Moan and P. Rudling, Eds., ASTM International, West Conshohocken, PA, pp. 400-426, 2002.

Bell W. L., Zirconium In Nuclear Applications, ASTM STP 551, ASTM, 199-200, 1974.

Bement A. L., Tobin J. C. and Hoagland R. G., "*Effects of Neutron Irradiation on the Flow and Fracture Behavior of Zircaloy-2*", Flow and Fracture, ASTM-STP 380, ASTM, 364-383, 1965.

Bossis P. Lelievre G., Barberis P., Iltis X. and LeFebvre F., "*Multi-Scale Characterisation of the Metal-Oxide Interface of Zirconium Alloys*", Proc. 12th Int. Symp. on Zr in the Nucl. Ind., ASTM-STP-1354, pp. 918-940, 2000.

Brun G., Pelchat J., Floze J. and Galimberti, M., Zirconium in the Nuclear Industry: Seventh Int'l Symposium, ASTM STP 939, Am. Soc. for Testing and Materials, Philadelphia, 597-616, 1987.

Causey A. R., "*In-reactor stress relaxation of zirconium alloys*", ASTM Spec. Techn. Publ. 551, pp. 263-, 1974.

Causey A. R., Fidleris V., MacEwen S. R. and Schulte C. W., "*In-reactor deformation of Zr2.5Nb pressure tubes*", ASTM Spec. Techn. Publ. 956, pp. 54-, 1988.

Causey A. R., Holt R. A., Christodoulou N. and Ho E. T. C., "*Irradiation-enhanced deformation of Zr-2.5Nb tubes at high neutron fluences*", Zirconium in the Nuclear Industry: Twelfth International Symposium, ASTM STP 1354, pp. 74-85, ASTM, West Conshohocken, PA, 2000.

Chalmers B., Physical Metallurgy, John Wiley and Sons, 1959.

Cheadle B. A., Ells C. E. and van der Kuur, J., "*Plastic Instability in Irradiated Zr-Sn and Zr-Nb Alloys*", Zirconium in Nuclear Applications, ASTM STP 551, American Society for Testing and Materials, 370-384, 1974.

Cheng B-C., Kruger R. M. and Adamson R. B., "*Corrosion Behaviour of Irradiated Zircaloy*", Proc. 10th Int. Symp. in the Nucl. Ind., ASTM-STP-1245, pp. 400-418, 1994.

Chow C. K. and Nho K. H. "*Effect of thickness on the fracture toughness of irradiated Zr-2.5Nb pressure tubes*", Journal of Nuclear Materials 246, 84-87, 1997.

Chow C. K., Coleman C. E., Koike M. H., Causey A. R., Ellis C. E., Hosbons R. R., Sagat S., Urbanic V. F. and Rodgers D. K. "*Properties of an Irradiated Heat-Treated Zr-2.5Nb Pressure Tube Removed From the NPD Reactor*", Zirconium in the Nuclear Industry: Eleventh Int'l Symposium, ASTM STP 1296, E. R. Bradley and G. P. Sabol, Eds., Am. Soc. For Testing and Materials, 469-491, 1996.

Chow C. K., Holt R. A., Woo C. H. and So C. B., "*Deformation of Zirconium Irradiated by 4.4 MeV Protons at 347 K*", Journal of Nuclear Materials 328, 1-10, 2004.

Coleman C. E. and Theaker J. R., "*Effect of Ingot Preparation Method on Irradiation Response of Zr-2.5Nb*", Proc. 14th ASTM Symposium on Zirconium in the Nuclear Industry, Stockholm, 2004.

Comstock R. J., Schoenberger G. and Sabol G. P., "*Influence of Processing Variables and Alloy Chemistry on the Corrosion Behavior of ZIRLO Nuclear Fuel Cladding*", Zirconium in the Nuclear Industry: 11th Int'l Symposium, ASTM STP 1295, E. R. Bradley and G. P. Sabol, Eds., American Society for Testing and Materials, pp.710-725, 1996.

Cox, B. and Rudling P., "*Hydriding Mechanisms and Impact on Fuel Performance*", Advanced Nuclear Technology for ZIRAT-5, 2000.

Cox B., "*Some Thoughts on the Mechanisms of In-Reactor Corrosion of Zirconium Alloys*", J. Nucl. Mater., 336, pp. 331-368, 2005.

Dahlbäck M., L. Hallstadius L, Limbäck M., Bunel, G., Moinard P., Andersson T., Askeljung P., Flygar J. and M. Karlsson, "*The Effect of Beta Quenching in Final Dimension on the Irradiation Growth of Tubes and Channels*", Proc. 14th ASTM Symposium on Zirconium in the Nuclear Industry, Stockholm, 2004.

Davies P. H., Hosbons R. R., Griffiths M. and Chow C. K., "*Correlation Between Irradiated and Unirradiated Fracture Toughness of Zr-2.5Nb Pressure Tubes*", Zirconium in the Nuclear Industry: Tenth International Symposium, ASTM STP 1245, A. M. Garde and E. R. Bradley, Eds., American Society for Testing and Materials, Philadelphia, 135-167, 1994.

Davies P. H. and Shewfelt R. S. W., "*Link Between Results of Small- and Large-Scale Toughness Tests on Irradiated Zr-2.5Nb Pressure Tube Material*", Zirconium in the Nuclear Industry: Eleventh International Symposium, ASTM STP 1295, E. R. Bradley and G. P. Sabol, Eds., American Society for Testing and Materials, 492-517, 1996.

deCarlan Y., Regnard C., Griffiths M., Gilbon D. and Lemaignan, C., "*Influence of Iron in the Nucleation of <c> Component Dislocation Loops in Irradiated Zircaloy-4*", Zirconium in the Nuclear Industry: 11th Int'l Symposium, ASTM STP 1295, E. R. Bradley and G. P. Sabol, Eds., American Society for Testing and Materials, 648-653, 1996.

APPENDIX A – Unit Conversion

TEMPERATURE

°C + 273,15 = K

°C*1,8 +32 = °F

T(K)	T (°C)	T(°F)
273	**0**	32
289	16	61
298	25	77
373	**100**	212
473	**200**	392
573	**300**	572
633	360	680
673	**400**	752
773	**500**	932
783	510	950
793	520	968
823	550	1022
833	560	1040
873	**600**	1112
878	605	1121
893	620	1148
923	650	1202
973	**700**	1292
1023	750	1382
1053	780	1436
1073	**800**	1472
1136	863	1585
1143	870	1598
1173	**900**	1652
1273	**1000**	1832
1343	1070	1958
1478	1204	**2200**

MASS

kg	lbs
0,454	**1**
1	2,20

DISTANCE

x (µm)	x (mils)
0,6	0,02
1	0,04
5	0,20
10	0,39
20	0,79
25	0,98
25,4	**1,00**
100	3,94

PRESSSURE

bar	MPa	psi
1	0,1	14
10	**1**	142
70	7	995
70,4	7,04	**1000**
100	10	1421
130	13	1847
155	15,5	2203
704	70,4	**10000**
1000	100	14211

STRESS INTENSITY

MPa√m	ksi√inch
0,91	**1**
1	1,10